Self-folding using capillary forces

Kwok, Kam Sang; Huang, Qi; Mastrangeli, Massimo; Gracias, David

DOI
10.1002/admi.201901677

Publication date
2019

Document Version
Final published version

Published in
Advanced Materials Interfaces

ADVANCED MATERIALS INTERFACES
www.advmatinterfaces.de

Self-Folding Using Capillary Forces

Kam Sang Kwok, Qi Huang, Massimo Mastrangeli, and David H. Gracias**

Self-folding broadly refers to the assembly of 3D structures by bending, curving, and folding without the need for manual or mechanized intervention. Self-folding is scientifically interesting because self-folded structures, from plant leaves to gut villi to cerebral gyri, abound in nature. From an engineering perspective, self-folding of sub-millimeter-sized structures addresses major hurdles in nano- and micro-manufacturing. This review focuses on self-folding using surface tension or capillary forces derived from the minimization of liquid interfacial area. Due to favorable downscaling with length, at small scales capillary forces become extremely large relative to forces that scale with volume, such as gravity or inertia, and to forces that scale with area, such as elasticity. The major demonstrated classes of capillary force assisted self-folding are discussed. These classes include the use of rigid or soft and micro- or nano-patterned precursors that are assembled using a variety of liquids such as water, molten polymers, and liquid metals. The authors outline the underlying physics and highlight important design considerations that maximize rigidity, strength, and yield of the assembled structures. They also discuss applications of capillary self-folding structures in engineering and medicine. Finally, the authors conclude by summarizing standing challenges and describing future trends.

1. Introduction

Fabrication and assembly methods that seek to shape and change the form and properties of materials are central to human life. With innovations such as Henry Ford's assembly line to Jack Kilby's integrated circuit, it has become relatively straightforward to assemble complex macroscale machines and miniaturized devices.[1] In contrast, while the integration and assembly of inherently 2D and stacked devices are relatively facile at small size scales, i.e., below about 1 mm, using very large scale integration (VLSI) processes,[2] it is extremely challenging to fabricate and assemble nonplanar, curved, and angled 3D structures with dissimilar materials. The challenge is rooted in several fundamental material and engineering constraints that are encountered at small size scales.[3–8] For example, due to large surface area-to-volume ratios, surface roughness, trapped charges, and local condensation, stiction increases significantly. Consequently, manipulation and release of cargo by robotic probes become challenging during and after release in pick-and-place assembly.[9] In addition, high-throughput and high-resolution imaging that is needed for optical feedback-based microcomponent placement and precision registration is extremely demanding for 3D robotic assembly. Hence, it is well accepted that new paradigms such as self-assembly are needed for 3D small scale manufacturing.[10]

Self-assembly is a biologically inspired methodology of assembling integrated devices by allowing smart designed components or parts to interact with each other via mobility provided by thermal energy, fluid flow, or other forms of mechanical agitation.[11] This concept was initially developed and investigated using noncovalent bonds and macromolecules within supramolecular systems[12] and was later adapted to non-molecular nano-, micro-, and even macro-scopic parts.[10,13–16] While self-assembly is often associated with programmed aggregation of many parts into organized structures, more recently, engineered bending, curving, and folding of micro- and nano-structures has been used to assemble 3D functional devices. This review concentrates on these types of self-assembly techniques that create organized structures by bending, curving, and folding, which we collectively refer to as self-folding. Specifically, this review only discusses self-folding using capillary forces, and the reader is directed elsewhere to excellent reviews on self-folding driven by alternate forces derived from the release of differential thin film stress or hydrogel swelling.[4,15,17–23]

While examining the forces that can be used for assembly at small size scales, it is evident that capillary forces offer several attractive characteristics. These forces can be applied across material classes and scale favorably at small length scales.

K. S. Kwok, Q. Huang
Department of Chemical & Biomolecular Engineering
Johns Hopkins University
3400 North Charles Street, Baltimore, MD 21218, USA
Dr. M. Mastrangeli
Electronic Components, Technology and Materials
Department of Microelectronics
Delft University of Technology
Feldmannweg 17, 2628CT Delft, Netherlands
E-mail: m.mastrangeli@tudelft.nl
Prof. D. H. Gracias
Department of Chemical & Biomolecular Engineering
Department of Materials Science and Engineering
Johns Hopkins University
3400 North Charles Street, Baltimore, MD 21218, USA
E-mail: dgracias@jhu.edu
The ORCID identification number(s) for the author(s) of this article can be found under https://doi.org/10.1002/admi.201901677.

DOI: 10.1002/admi.201901677

There is significant evidence for the widespread use of capillary forces in nature (**Figure 1**). A nonexhaustive list of examples includes the superhydrophobicity of plant leaves such as the lotus leaf and rose petals[24,25] with varying degrees of adhesion,[26] transpiration-driven inner liquid flow, and the so-called cohesion-tension mechanism in plants,[27,28] transportation of water droplets on cactus spines (Figure 1a),[29] actuation and blooming in some flowers,[30,31] capillary food transport in the beaks of shorebirds (Figure 1b),[32] actuation of the hummingbird's tongue,[33,34] condensation of bird feather bundles,[35] adhesion of tree frog toe pads (Figure 1c)[36] and of insect setae,[37] jumping[38] and locomotion of water striders (Figure 1d),[39–41] breathing of underwater insects and spiders,[42] designs of spiral bundles in spider webs,[43,44] collapse of lung airways,[45,46] deformation of blood vessels,[47] and elastocapillary instability in mitochondrial fission.[48]

2. Theoretical Considerations and Relevant Parameters

2.1. Force Scaling

Forces that are used to perform functional engineering tasks scale with size. While multiple forces exert tangible effects at a given physical scale, the hierarchy of the magnitude of forces is scale specific. Relative magnitude is particularly important as one approaches the sub-millimeter scales. At these small scales, forces that scale with volume, such as gravity, inertia, and magnetic force, or those that scale with area, such as elastic forces, become less relevant as compared to surface tension, which scales with length (**Figure 2**a). This favorable relative scaling of capillary forces makes them dominant at micro- and nano-scales, and justifies the wide adoption of surface tension for the (self-)assembly and actuation of micro- and nano-structures (Figure 2b).[49] It is noteworthy that to date, 3D cubic and pyramidal nanoparticles with sizes as small as 100 nm and precisely defined functional facets with 15 nm resolved lithographical patterns in all three dimensions can be fabricated only by capillary self-folding.[50] Since capillary assembly can be used up to self-fold lithographically patterned (inherently 2D) precursors all at once, the process can be highly parallel and applied at wafer-scale, which is important for cost-effective batch manufacturing of 3D micro- and nano-structures. For example, 2D precursors for solder hinge-based capillary assembly can be patterned in parallel using photo- or nanoimprint-lithography, self-folded after release from the wafers en masse by heating, and even aggregated to form larger self-assembled devices (Figure 2c). Also, there is significant versatility as the self-folding process is fairly material agnostic. Indeed, hydrogels and even atomically-thin 2D materials, such as graphene and molybdenum disulfide (MoS_2), were recently self-folded into microscopic polyhedral structures using capillary forces.[51–54]

2.2. Surface Tension

Surface tension quantifies the free energy associated with interfaces that separate immiscible phases of matter. Surface tension subtends the tendency of interfaces to minimize their area and thus resist deformation, expansion, compression, cutting, spreading, and other perturbations. Surface tension arises from a local imbalance in intermolecular forces at the interface between different materials or material phases.[56] Due to the

Kam Sang Kwok received his B.S. from the University of Illinois at Urbana-Champaign in 2013. He is currently a Ph.D. student at the Johns Hopkins University working on manufacturing self-folding nanostructures.

Massimo Mastrangeli is a tenure-track assistant professor at TU Delft's ECTM laboratory, where he develops silicon/polymer-based organ-on-chip and nanoparticle-based devices. Prior to joining TU Delft, Dr. Mastrangeli held research appointments at the Max Planck Institute for Intelligent Systems (Stuttgart, Germany) for soft microrobotics and granular matter, at the Universite' Libre de Bruxelles (ULB, Belgium) for micromechanics and capillary micromanipulation, at École Polytechnique Fédérale de Lausanne (EPFL, Switzerland) for micro/nanofabrication and distributed robotics, and at imec Belgium (Leuven, Belgium) for fluidic microsystems integration and microelectronic packaging. Dr. Mastrangeli holds a B.Sc. and M.Sc. degree (both cum laude) in Electronic Engineering from University of Pisa (Italy) and a Ph.D. degree in Materials Engineering from University of Leuven (Belgium).

David H. Gracias is a professor at the Johns Hopkins University. He received his Ph.D. from the University of California at Berkeley in 1999 and did postdoctoral work at Harvard University, all in chemistry or related fields. His independent laboratory, since 2003, has pioneered the development of self-folding methods and assembly paradigms for 3D micro-, nano-, and bio-devices.

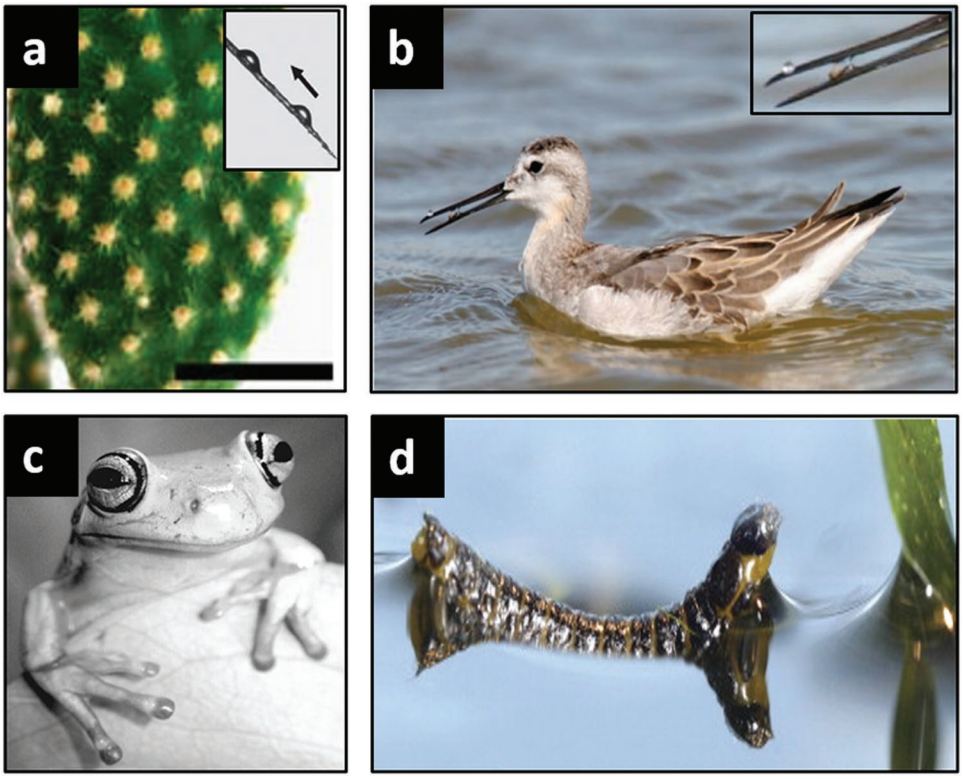

Figure 1. Examples of the use of capillary forces in nature. a) Photograph of *Opuntia microdasys*, a flowering plant in the cactus family with well distributed, centimeter spaced clusters of spines and trichomes. The inset shows water drops from fog that are driven from the tip to the base of a spin at a tilt angle of –45°; capillary forces are involved in this transport. Reproduced with permission.[29] Copyright 2012, Springer Nature. b) Photograph of a juvenile Wilson's phalarope (*Phalaropus tricolor*) feeding. The transport of prey from the tip of the beak to the mouth of the bird involves a surface tension mechanism. The inset shows the prey suspended in the droplets trapped in its beak. Reproduced with permission.[32] Copyright 2008, the American Association for the Advancement of Science. c) Photograph of a white tree frog (*Litoria caerulea*) capable of attaching to smooth surfaces using toe pads that utilize a combination of forces including surface tension. Reproduced with permission.[36] Copyright 2006, Royal Society. d) Photograph of a *Pyrrhalta* beetle larva that arches its nose and tail to drive up water menisci using surface tension. Reproduced with permission.[40] Copyright 2007, Elsevier.

interfacial discontinuity, cohesion among molecules belonging to the same phase manifests as a net force tangential to the interface.[57] The force-based interpretation of surface tension, accordingly measured as force per unit length (i.e., N m^{-1} in SI units), is equivalent to the energy-based interpretation stemming from Gibbs' thermodynamic derivation of surface tension as the variation in excess surface energy upon perturbation of surface area[56]—hence the equivalent measure of surface tension in J m^{-2}. Surface tension is related to solid interfacial energy, surface stress,[58] and work of adhesion,[59] and is equivalent to surface free energy only for one-component liquids.[57] By the same token, surface tension is most commonly referred to liquids, i.e., to liquid/liquid or liquid/gas interfaces in particular.

Capillary phenomena are ubiquitous in natural (see Introduction) as well as in artificial domains: clumping of wet hair,[60] drops and bubbles, evaporation, capillary rise, jet instabilities, liquid-based cleaning and wetting are some manifestations familiar from time immemorial.[24] In spite of this, the scientific concept of surface tension was first introduced only in the 17th century,[57] and the earliest scientific studies and models of capillarity and surface tension-related phenomena date back only to little more than two centuries ago—eminently through the works of Young, Laplace, Poisson, and Plateau.[24,55] Scientists and engineers active in micromechanics and nanoengineering may have first-hand experience with properties and effects of liquid surface tension, i.e., capillarity, if only because of, e.g., liquid coatings, cleaning and drying of substrates, bubble formation in microchannels, component soldering or self-assembly,[61] capillary coalescence of micro- and nano-structures,[62–64] or stiction issues[65–67] upon release of suspended micro-electromechanical systems (MEMS) structures.[68]

2.3. Forces and Torques

When considering finite liquid volumes—as is the case for droplets and liquid bridges of specific interest here—two components which make up the total capillary force need to be distinguished (Figure 2b).[55,61]

The surface tension force component is always tensile and acts at the triple contact line, i.e., the 1D interface among three adjacent phases (e.g., the border of a liquid (L) droplet sitting on a solid (S) substrate surrounded by vapor (V) or another (immiscible) liquid). The orientation of the force (per unit length) at the contact line ensues from the local balance of the interfacial tensions associated with the three interfaces (i.e., liquid/solid (LS), liquid/vapor (LV), and solid/vapor (SV)

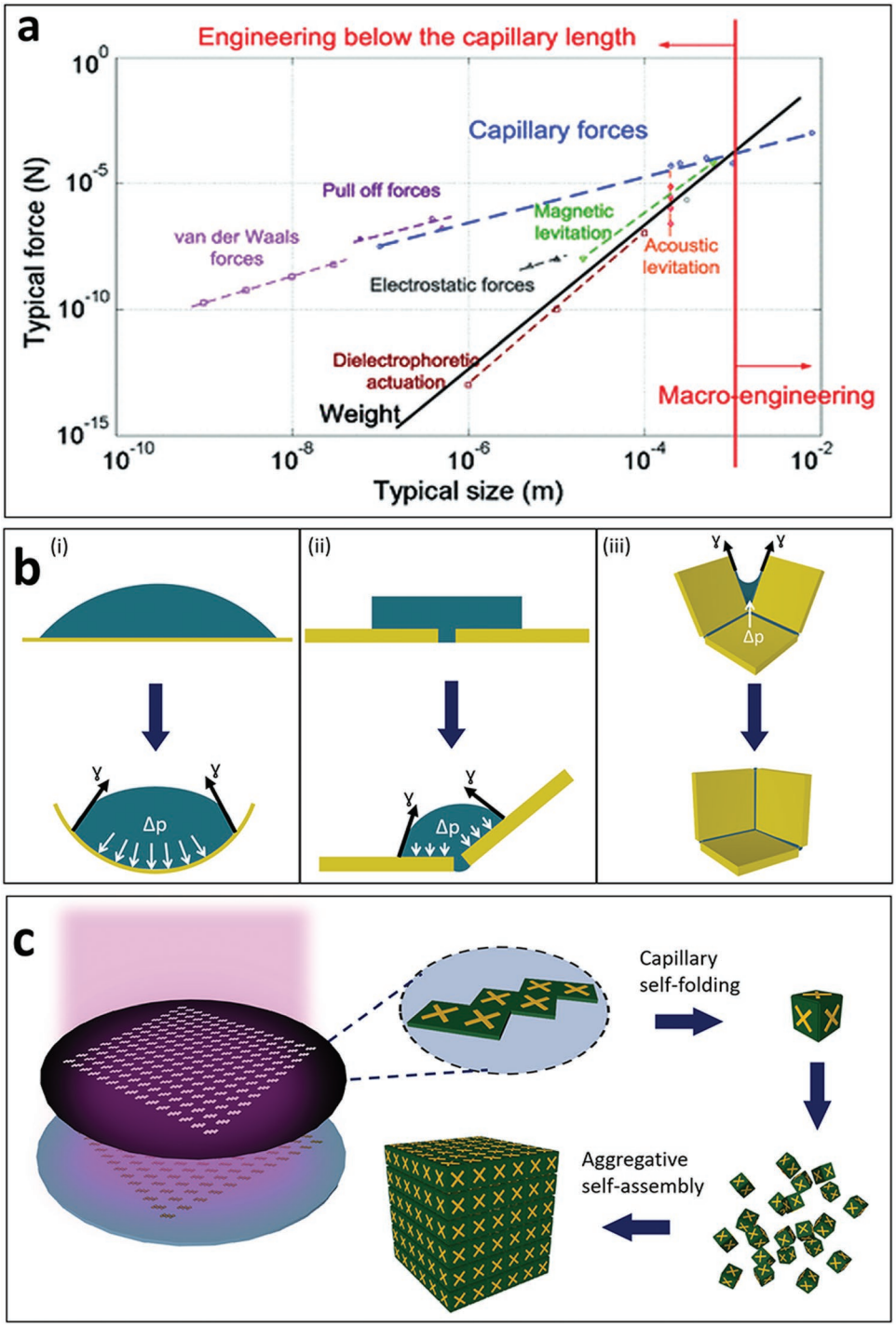

Figure 2. Assembly using capillary forces. a) Graph showing the relative magnitude of forces as a function of size on a log–log scale. All the points represent different experimental data and the dashed straight lines represent scaling laws. Reproduced with permission.[55] Copyright 2013, Springer Nature. b) Schematics of the role of surface tension (γ) and net capillary pressure (Δp) in capillary self-folding. i) Capillary self-folding of a soft membrane. ii) Capillary self-folding of rigid hingeless panels. iii) Self-alignment of locking hinges during capillary self-folding. c) Conceptual illustration of the highly parallel and hierarchical capillary assembly paradigm compatible with wafer-scale fabrication. Large numbers of 2D precursors can be patterned using photolithography, and self-folded in parallel in a single step to assemble polyhedral building blocks. Such building blocks can potentially be further self-assembled by aggregation to form 3D microarrays and metamaterials with well-defined patterns in all three dimensions.

interfaces in the example above). Such balance is captured by the Neumann relation, notably for liquid/liquid interfaces (e.g., droplets floating on liquid beds) and for liquids resting on very soft substrates.[59] For droplets sitting on substrates whose rigidity makes the force component normal to the substrate inconsequential (i.e., Young's modulus $E \rightarrow \infty$), the

interfacial force balance at the triple contact line can be simplified and is typically expressed via the horizontal projection of the Neumann force triangle, better known as the Young–Dupré equation $\gamma_{SV} = \gamma_{SL} + \gamma \cos\theta$. The Young–Dupré equation inherently defines the (static) liquid contact angle θ, a macroscopic though imprecise quantification of liquid affinity to the substrate;[69] in particular, lyophobic (lyophilic) substrates are evidenced by contact angles larger (smaller) than 90°, whereas perfect wetting is achieved for $\theta \to 0^{\circ}$.

The second component of the capillary force arises from the pressure difference Δp across the liquid interface, whereby the ensuing surface curvature is supported by the surface tension. Described by the Young–Laplace equation $\Delta p = 2H\gamma$, this force component (of value equal to $A\Delta p$, arising from net pressure impinging on a liquid/solid contact area A) can be either tensile or compressive depending on the positive or negative sign of the mean curvature H of the capillary interface (e.g., the mean curvature is $1/r$ and $1/2r$ respectively for spheres and cylinders of radius r).

Both surface tension and Laplace components of the total capillary force scale linearly with length, and they are proportional to the surface tension coefficient γ (e.g., in air and at room temperature: water, 72 mN m^{-1}; ethanol, 22.4 mN m^{-1}; hexadecane, 27.6 mN m^{-1}; liquid metals > 400 mN m^{-1}; refer to[70–72] for comprehensive lists of values of γ). The surface tension coefficient of a given liquid is additionally dependent on temperature and concentration of solvents, particularly of surface-active species (i.e., surfactants). Gradients of surface tension can be locally induced by temperature gradients, surfactant concentration gradients, or by liquid mixtures, and they can promote transient interfacial flows[24,73] and hydrodynamic instabilities.[74] As a consequence, the total capillary force depends on liquid surface tension, liquid-to-substrate affinity (contact angle), liquid volume, and geometrical and environmental boundary conditions. All these are parameters that can be leveraged to tune magnitude, orientation, and sign of the capillary force when designing capillary self-folding structures.

For a given liquid density ρ and surface tension γ, the (gravito)capillary length $L_C = \sqrt{\gamma/\rho g}$ defines the size range below which capillarity dominates gravitational effects, including weight of objects and hydrostatic pressure. In this size range (e.g., below ≈2.7 mm for water at room temperature), the capillary force can additionally become comparable and even larger than the shear and/or bending stiffness of soft materials. As a result, capillary forces can microscopically deform soft substrates in close proximity of contact lines;[75] and capillary torques can macroscopically bend or fold unconstrained substrates larger than a corresponding (bending) elastocapillary length $L_{EC} \approx \sqrt{B/\gamma}$ ensuing from the ratio of bending stiffness B and surface tension.[59,76,77] For the common case of a curved sheet or membrane of thickness t and Poisson's ratio ν, $B = Et^3/12(1-\nu^2)$. Under the rubric of elastocapillarity,[59] the latter effects are relevant for the micromechanics and applications of self-folding reviewed below. It is worth noting that substrates with high degree of softness (i.e., $E < 10$ kPa, typically polymeric or gel-based) or small bending compliance (including atomically thin ones[54]) became of wide interest and utility only recently, i.e., long after the earliest demonstrations of engineered microscale self-folding, which involved rigid substrates with well-defined folding lines. Suffice to mention that the work of Py et al.[78] that first described analytically the shape of elastocapillary-folded continuous strips and voxels appeared about 25 years after the important demonstrations by Syms and colleagues of capillary self-folding of micro-(opto-) electro-mechanical systems (M(O)EMS).[72,79] The historical development of self-folded microstructures followed a different path from the conceivable logical sequence sketched in **Figure 3** that is outlined in the following section.

3. Types of Capillary Self-Folding

3.1. Elastocapillary Folding and Self-Wrapping

Py et al. described how millimeter-sized voxels with roughly the shape of a polyhedron (e.g., a tetragon) can be self-folded by placing a liquid droplet of commensurate volume (less than 80 µL) on a thin (40–80 µm), elastic, unconstrained, continuous and mildly lyophilic sheet (made of polydimethylsiloxane (PDMS) in their case) with appropriate shape (e.g., a triangle) and of linear size larger than the bending elastocapillary length of the liquid/substrate pair.[78] Under these conditions, the thin film adheres to and spontaneously self-wraps around the droplet (Figure 3i). The folding is cumulatively driven by the energetically favorable wetting of the lyophilic sheet surface by the droplet, whose capillary pressure applies a distributed bending deformation to the substrate, and by the (localized) bending torque associated with the tensile surface tension force insisting on the triple contact lines, which pulls the substrate inwardly (Figure 2bi). During the folding and as the liquid evaporates, the liquid/air area decreases while the elastic energy increases due to sheet bending. Py et al. showed semi-analytically that the ratio of bending and surface energies determines the radius of curvature of the capillary folding, of the order of L_{EC}, and that the critical dimension for folding L_{crit} is proportional to L_{EC} by a shape-dependent coefficient S, i.e., $L_{crit} = SL_{EC}$. They also reported that several bending modes and wrapping states of different degree of stability can be distinguished depending on sheet shape, sheet size relative to L_{EC} and droplet volume. Instead of reaching a maximum bending before reopening as the liquid volume decreased, sufficiently thin sheets eventually encapsulated the evaporating droplet fully, forming a closed voxel with morphology dependent on sheet shape. Later experimental and theoretical work by de Langre et al. confirmed the switching among different modes of capillary folding, and additionally pointed to a transition from folded to unfolded state due to dewetting (i.e., unpinning of the droplet from the edges of the substrate) during elastocapillary wrapping of a flexible membrane.[80] The latter observation was echoed by further studies based on 2D[81] and simplified 3D[82] models, according to which contact line unpinning should lead to a premature unfolding of the sheet compared to the pinned case and consequently to an overestimation of L_{crit}. Based on the model by Py et al., recent experimental work by Bae et al. showed that capillary self-folding can be conversely used to estimate L_{crit} and from that, all other parameters being known, to determine with fair accuracy the elastic modulus of thin sheets of a variety of materials, ranging from soft ($E \approx$ kPa, e.g. hydrogels (pNIPAM,

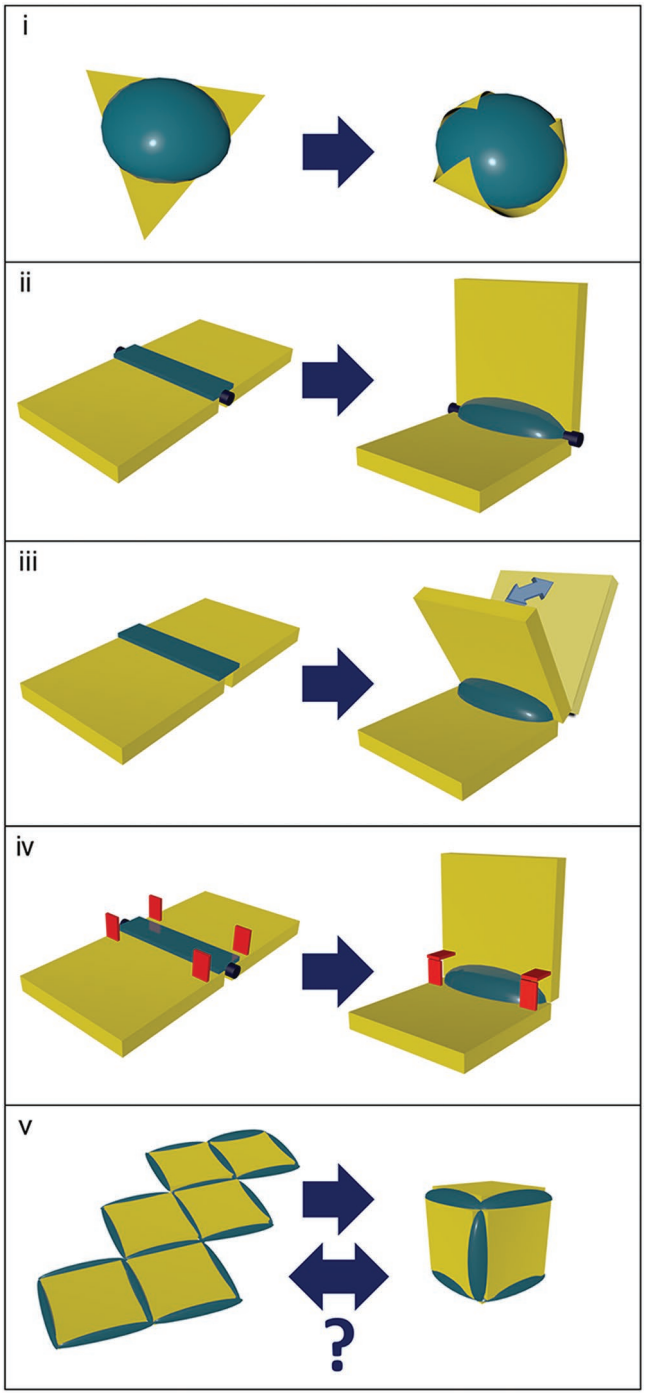

Figure 3. Classification of capillary self-folding mechanisms. i) Elastocapillary folding of continuous soft substrates around droplets (i.e., self-wrapping). ii) Self-folding with mechanical hinges. iii) Hingeless self-folding with multiple energetically equivalent final states. iv) Hingeless self-folding with mechanical locking. v) Hingeless self-folding with capillary locking, capillary self-alignment, and potential dynamic reversibility.

polyacrylamide) and polyimide) to stiff ($E \approx$ GPa, e.g. glassy polymers (PpMS)).[52] They also gave substantial experimental confirmation of the theoretical values of S for triangular (7.0) and square-shaped sheets (11.9),[78,82] as well as of the independence of S from the value of the liquid contact angle. Using a droplet of ferrofluid on a thin triangular PDMS membrane, Jamin et al. described additional anisotropic shapes for capillary origami and evidenced an overturning morphological instability under the competing effects of elasticity, gravity, and an external magnetic field.[83] Gao and McCarthy further noted that sufficiently thin substrates of materials normally considered hydrophobic also self-wrap around droplets,[84] pointing to the distinct role of liquid adhesion and wetting in the process.[85] Along the same line, Geraldi and coworkers showed theoretically and demonstrated experimentally how rigid topographic structures,[86] and particularly a roughening hydrophobic coating making smooth surfaces superhydrophobic,[87] can completely suppress capillary self-folding of thin soft sheets.

A few comments are in order here. First, on a continuous and smooth elastic substrate with unpatterned folding lines, pivot axes for capillary torque are not well defined and may depend on the exact initial placement of the droplet on the substrate, as well as on the kinetics of droplet deposition.[82] In view of this, pinning of the droplet on all edges of the sheet is recommended to avoid partial or nonreproducible results, particularly in case of partial liquid wetting. By the same token, upon liquid deposition on a substrate in air, the edge of the substrate topographically confines the liquid within its perimeter.[62] Second, Gauss' Theorema Egregium implies that conformal wrapping of planar surfaces, such as flat sheets, around nonplanar ones, like the surface of hemispherical droplets, cannot be achieved unless stretching and bending (as in origami-inspired structures[20]) and/or cuts (as in kirigami[88]) are included in the wrapping structure. Therefore, droplet self-wrapping necessarily involves stretching as well as bending of the substrate; conversely, continuous substrates can be tailored with cuts to achieve predetermined self-wrapping into 3D spheroidal shapes and thus maximize the ratio of surface to enclosed volume.[78,89–91] Third, downscaling benefits elastocapillary folding, since L_{EC} scales with sheet thickness t to the power of 3/2 and thinner substrates are associated with smaller critical lengths. Hence, 10–100 nm-sized nanostructures can conceivably be self-folded out of atomically thin sheets.[54] Fourth, closure of the voxel requires partial evacuation of the inner liquid (i.e., volume shrinking), which may take place by means of evaporation (e.g., water in air) or by dissolution in a solvent (e.g., chloroform in water[54]). Fifth, even upon full closure the voxel is hardly sealed, and in the absence of strong adhesion (due to, e.g., stiction, dissolved impurities or van der Waals interactions[92]) let alone mechanical fixation, the folding of the voxel is only temporary: if the bending energy exceeds the adhesion energy, the voxel unfolds upon full evaporation of the droplet and final drying of the substrate.

3.2. Hinged and Hingeless Folding Lines

Predefinition of folding lines is crucial for predictability and repeatability of capillary self-folding. As importantly, in the design of self-folding 3D structures the introduction of folding lines goes along with the decomposition of the inherently polyhedral target structure into a single, planar polygon referred to as the net.[93] The 2D net is composed by the faces of the

target polyhedron simply connected within a single plane. The decomposition of a polyhedron into an associated net is typically nonunivocal though nonarbitrary. A folding line interlocks a pair of adjacent and nonoverlapping polygonal panels of the net and functions as pivot for their out-of-plane motion (Figure 2bii and Figure 3ii). Capillary self-folding can in this case still be incepted by placing and confining a liquid droplet over the full lyophilic net.[92,94] Legrand et al. integrated a microfluidic system in their micromachined substrate for controlled in situ delivery of liquid droplets within self-folding voxels.[95] They later developed a 3D micromachining process involving corner lithography that allowed the fabrication of silicon nitride-based capillary self-folding structures with stop-programmable hinges, i.e., hinges whose geometry could precisely impose a predesigned final folding angle, and whose low rigidity could enforce the mechanical stability of the self-folded structures.[96] Honschoten et al. devised a 2D analytical model of the evolution of the capillary self-folding of a tetrahedral voxel from a hinged net of triangular, surface micromachined microplates.[92] Their model predicted equilibrium states as a function of the enclosed liquid droplet volume. By matching the model with experimental data, Honschoten et al. could predict in particular partial closure of the voxel under specific conditions related to the stiffness of the substrate, as well as, in the case of partial substrate wetting by the liquid, the maximum achievable out-of-plane rotation of the plates as a function of the (finite) contact angle.[92]

A single liquid droplet wetting the full net, and filling almost the entire voxel after its deployment, is sufficient under conducive conditions for capillary self-folding,[97] but nevertheless not necessary. Rather, as first demonstrated by Gracias and colleagues, the surface tension of smaller liquid droplets distributed over the net can be exploited to pull locally on each side of the net's folding lines and drive the self-folding. Syms and Yeatman first showed the feasibility of pairs of adjacent, rotating planar microfabricated structures turning into articulated, out-of-plane 3D architectures by capillary self-folding.[79] They locally deposited and/or lithographically patterned pads made of glass,[98] polymers,[99] and especially solder[79] across the hinges linking adjacent panels, and then proceeded to thermal reflow to obtain confined liquid interfaces out of those materials (free of oxide, in case of solder). They could show that surface tension of the molten pads drove the self-actuation of the suspended, surface micromachined structures out of the substrate plane.

Syms and Yeatman also developed an analytical 2D model of the process, which they solved numerically[79] and then analytically.[100] Assuming a cylindrical shape for the free molten pad surface of initial height h and width $2w$ and neglecting all but capillary forces, they derived closed-form expressions for surface energy and capillary torque as a function of two angles, defining respectively the cylindrical section spun by the pad and the out-of-plane rotation of the hinged panel. The model predicted in particular that the final rotation angle could be controlled by the initial normalized height of the pad $\eta = h/w$ for $\eta > 0.25$: the unconstrained hinged panel would rotate from the horizontal until the final position, which corresponded to the minimum of surface energy and null capillary torque. Through their model, Syms et al. could account for several process and material parameters, including the maximum breadth of the panels (of the order of L_C) that could in principle be lifted,[72] confirming the specific benefit of capillary self-folding for sub-millimeter-sized structures. This modeling approach was later substantiated by finite-element quasistatic simulations, typically performed using the Surface Evolver[101] mathematical software. Such simulations could account for more realistic conditions, including fully 3D pad geometries[102,103] and a range of substrate and hinge materials as well as panel sizes and weights.[103,104] The predictions of these numerical models were closely matched by experimental data. In particular, relatively small differences with theory on equilibrium angles were mainly caused by imprecise control over the volume of deposited liquefiable material;[72] and though only by assuming bulk material properties and by neglecting dewetting, phase segregation, formation of intermetallics and other diffusional effects, capillary self-folding driven by molten solder was predicted to work down to nanosized structures,[103,104] as later confirmed experimentally.[50] To complement the quasistatic analyses, a model of the dynamics of the capillary folding process was also devised by Syms and colleagues, whereby the driving capillary torque was counteracted by air drag and viscous damping due to the hinge.[72] Whereas air damping was shown to be practically negligible, viscous damping turned out to be largely dependent on pad material. Video recordings of surface tension-driven M(O)EMS self-folding measured assembly times of the order of seconds and minutes respectively for solder,[100] and glass-based hinges,[98] the latter using rapid heating to temperatures above 1000 °C, whereas time-to-assembly was many minutes for polymer-based hinges at low temperature.[99]

Moving forward, Syms and colleagues realized that bending or deforming by capillary means elastic hinges linking fixed and moving panels in their microstructures would be problematic due to the quadratic scaling of elastic forces with size; moreover, by omitting hinges a second free surface must exist in the gap between the panels, causing an additional force on the panels that would itself keep the gap closed and prevent detachment of the panels away from the rotation axis.[72] In addition, similar capillary self-folding results as with hinged panels could be expected in the absence of structural links, as the torque was not affected.[100] Hingeless 3D capillary self-folding (Figure 3iii) consequently received significant attention and became rapidly common.[72] However, energetic considerations also evidenced a limit in the accuracy and predictability of the final construction. All orientations of the moving panel with respect to the fixed horizontal panel insisting on a solid angle smaller than 90° were shown to possess the same free-boundary lengths and liquid cross-sectional areas, i.e., the same energy. Hence all these states are only marginally stable, and no barrier prevents further rotation upon reaching equilibrium.[100]

3.3. Mechanical Locking, Self-Alignment, and Reversible Folding

To avoid the previously mentioned inconvenience and make capillary self-folding more robust though at the expense of increased design complexity, Syms and colleagues introduced the use of solid mechanical limiters. They defined end-stops to stabilize target orientations for hingeless structures by hard

contact locking between adjacent panels (Figure 3iv).[99,100] More generally, mechanical locking provides two major advantages: 1) it allows folding structures to retain a nonzero driving capillary torque throughout their rotation, particularly including the predetermined final state since the rotation can be arrested before the energy minimum is reached (a similar concept[105] is used also for accurate capillary self-alignment in flip-chip assembly, mentioned below); and 2) it enables the process to be determined by precise lithography and etching rather than by the less controllable volume of reflowable material only. Higher assembly yield could be demonstrated this way, along with higher positional (sub-micrometric error) and orientational accuracy (minutes of arc).[106] Further along this line, mechanical limiters enabled actuation of more complex structures, featuring multiple elements interconnected by both active and passive links that could be actuated simultaneously or sequentially.[106,107] Mechanical locking additionally yielded 3D folded M(O)EMS with enhanced thermal and inertial stability.[108]

In developing hingeless self-folding geometries it was observed that the gap closing capillary force contributed to eliminate any clearance between adjacent panels. An ingenious further step along this direction was introduced by Gracias and colleagues through the use of the reflowing material as error-correcting besides mechanical locking resource for adjacent self-folding panels (Figure 2biii and Figure 3v).[103,104] They patterned reflowing material (polymer or solder) along the unconnected edges of the polygonal panels in the nets besides across the hingeless folding lines, so that upon mutual contact the panels would self-align while completing the self-folding into a voxel. Locking using liquid solder droplets that solidify after cooling allowed in addition the structures to be permanently bonded. This precise locking of the panels into the intended final geometry was enabled with much higher tolerance to initial conditions and process contingencies. Consequently, even with approximate dimensions, complex polyhedral shapes could be formed.[109] It is noteworthy that at small size scales the high surface tension of molten solder resists breakage even during tumbling of components, as evidenced in 3D solder-mediated aggregation of blocks used to build artificial crystals and 3D networks.[14,110] Attachment of parts using solder pads or bumps is also commonly used in flip-chip assembly and packaging,[111–113] with the added benefit of enhanced registration accuracy due to capillary self-alignment effects.[61]

Subsequent studies in self-aligning liquid hinges deposited at the periphery of polyhedra enabled design of error tolerant nets and control over folding pathways.[93,114–116] It is noteworthy that multiple arrangements and connections of polygons on nets are possible while folding a polyhedron. The number of nets increases exponentially with the number of faces of the polyhedron. For example, the tetrahedron has 2 nets, the cube and the octahedron have 11 nets, the dodecahedron and icosahedron have 43 380 nets, and the truncated octahedron has ≈2.3 million nets.[93] Meanwhile, assembly yields can vary dramatically with the type of net. Depending on the type of net, measured yields for perfect polyhedral self-folding with no visible defects ranged from 0% to over 35%.[93] By using capillary forces for self-folding of panels and self-alignment of hinges, one can capture biomolecular mimetic self-assembly processes and uncover design rules for high-yield nets (see next section).

Whereas the development of capillary M(O)EMS self-folding did not follow the conceivable derivation outlined above for presentation purposes, it is tempting to hypothesize what the next important achievements in capillary self-folding might be. We think that this will possibly have to do with adding dynamics and particularly reversibility to self-folded structures (Figure 3v)—akin to what has been already demonstrated in the same or similar contexts using alternative means, such as shape-memory polymers,[117] electrowetting[90,118] and swelling,[119,120] as well as chemical,[121] thermal,[122] thermochemical,[123] and thermomagnetic stimuli.[124] Achieving reversible self-folding exclusively by capillary forces is in principle feasible, not only via fluid substitution, as recently demonstrated by Wong et al. in their mimosa-inspired origami structures,[125] but also through the use of fluids with switchable surface tension (i.e., liquid metals such as Ga or In-based alloys,[126] or liquids employing switchable surfactants[127–131]), or the possibility of reverting the sign of the Laplace component of the total capillary force by modifying the curvature of the fluid interface(s).

4. Geometry and Path Design Rules

The geometry and arrangements of 2D precursors and panels can be used to manipulate capillary self-folding pathways, final 3D shape, and yield. For continuous precursor sheets, the aspect ratio, symmetry and surface area provide a means to achieve control. Following on the work of Py et al.,[78] Guo et al. fabricated 5 mm-sized triangular and square silicone sheets with a thickness of 1.25 μm. Upon water evaporation, they observed that although folding started at the vertices for both the triangular and square shapes, the triangular sheet self-folded into a hollow tetrahedral pyramid, while the square sheet folded into a cylindrical shape rather than a square pyramid (**Figure 4**a).[89] The authors rationalized this observation by noting that square sheets had longer folding characteristic lengths as compared to triangular sheets. Li et al. later used the mechanics of tapered beams to develop a generalized mechanical model of capillary self-folding of thin sheet precursors, which included triangular and square shapes as basic and particular cases.[132] They derived an analytical folding parameter of the form $\alpha_{\text{eff}} = \alpha_{\text{int}} \left(\frac{\gamma L^2}{Et^3} \right) S$ valid for any patterned sheet of characteristic length L and specific intrinsic factor α_{int}, and proposed a folding criterion based on the comparison of α_{eff} with an experimentally determined critical value α_{crit} dependent on material and geometrical properties.

At the nanoscale, Cho et al. observed that capillary deformation of annular nickel structures driven by thermal reflow of tin can result in different final morphologies,[133,134] such as wrinkled, saddled or wedged, based only on the varying width of the annulus (Figure 4b).[135] Likewise, tapered cantilever precursors were self-folded into spiral like 3D nanostructures with varying radii of curvature based on the angle of taper.[136] The width of the base of the cantilevers was larger than that of the tips, resulting in a larger area of the moment and larger radius of curvature at the base as compared to the tips (Figure 4c).

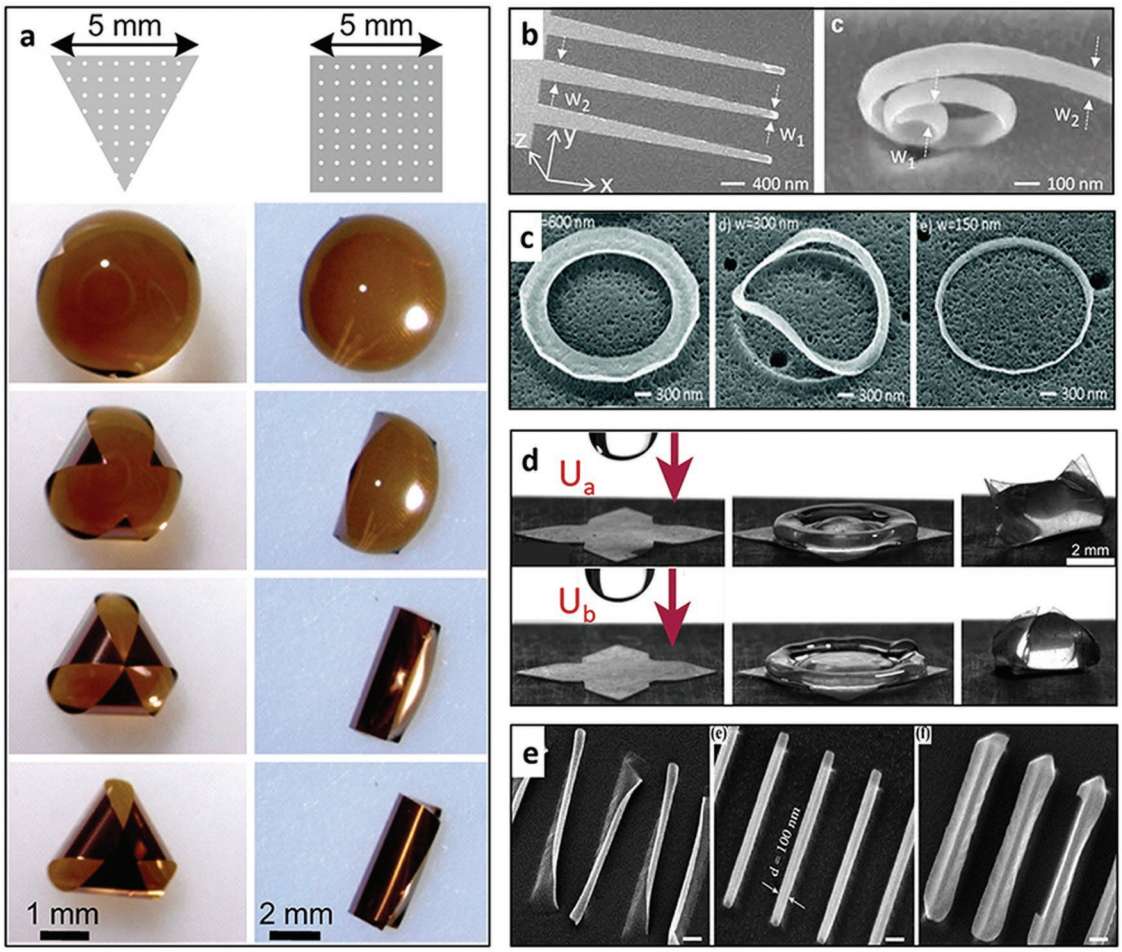

Figure 4. Geometric design and assembly rate considerations of capillary self-folding of continuous structures. a) Spontaneous folding (self-wrapping) of triangular and square silicone sheets illustrating that assembly can occur from vertices or sides based on the geometry. Reproduced with permission.[89] Copyright 2009, National Academy of Sciences. b) Scanning electron microscope (SEM) image of tapered cantilevers (i.e., $W_1 < W_2$) that self-fold with varying radii of curvature due to a varying area moment of inertia, resulting in the formation of a nanospiral. Reproduced with permission.[136] Copyright 2010, Wiley-VCH. c) SEM images of a wrinkled, saddled, and wedged nanostructures that self-fold from annuli with different widths. Reproduced with permission.[135] Copyright 2010, American Chemical Society. d) Optical images of a flower-shaped precursor forming different self-folded structures based on the impact velocity of a droplet of water. Reproduced with permission.[82] Copyright 2011, National Academy of Sciences. e) SEM images illustrating the effect of vertical-to-horizontal etch rate ratio of the underlying layer on capillary self-assembly of tube structures. Scale bar represents 200 nm. Adapted under the terms of a Creative Commons Attribution 4.0 International License.[137] Copyright 2017, The Authors, published by Springer Nature.

Liquid deposition and substrate preparation are also important parts of capillary self-folding-based fabrication processes (see Section 3.1). Concerning surface wetting and liquid deposition on precursors, Antkowiak et al. showed that a PDMS flower-shaped sheet folded into a pyramid after a drop of water impacted the sheet at a velocity of 0.92 m s^{-1} (Figure 4d), whereas reducing the velocity to 0.68 m s^{-1} caused it to form a cylindrical shape.[82] The researchers observed that the higher velocity allowed the water droplet to spread across the entire surface of the precursor, whereas the lower velocity drop wet the PDMS surface only partially, causing the final shape to be different.

Elsewhere, different self-folded shapes could be formed in metal reflow-based capillary self-folding by controlling the direction of plasma etching of the underlying sacrificial layer. Specifically, Dai et al. controlled the degree of anisotropy of plasma etching by varying the ratio of oxygen to tetrafluoromethane (O_2/CF_4) gas flow rate and observed both uniform and irregular self-folded nickel and tin rectangular nanopatterns (Figure 4e).[137] With a vertical-to-horizontal etch ratio of ≈1, irregular self-folded nanostructures were formed due to rapid etching of the substrate, quick release of the precursors and insignificant grain coalescence. In contrast, by increasing the etch ratio to ≈1.2, uniform tubes could be formed. When the vertical-to-horizontal etch ratio was increased further to ≈1.8, melting of Sn became significant even prior to the release of the precursors and the rectangular patterns collapsed.

In terms of design criteria for capillary self-folding of polyhedra, Gracias and Menon and coworkers discovered optimal self-folding nets using a combination of experiments and mathematical analyses.[93,114–116] They found that high yielding self-folding of polyhedra occurs with compact nets with low radius

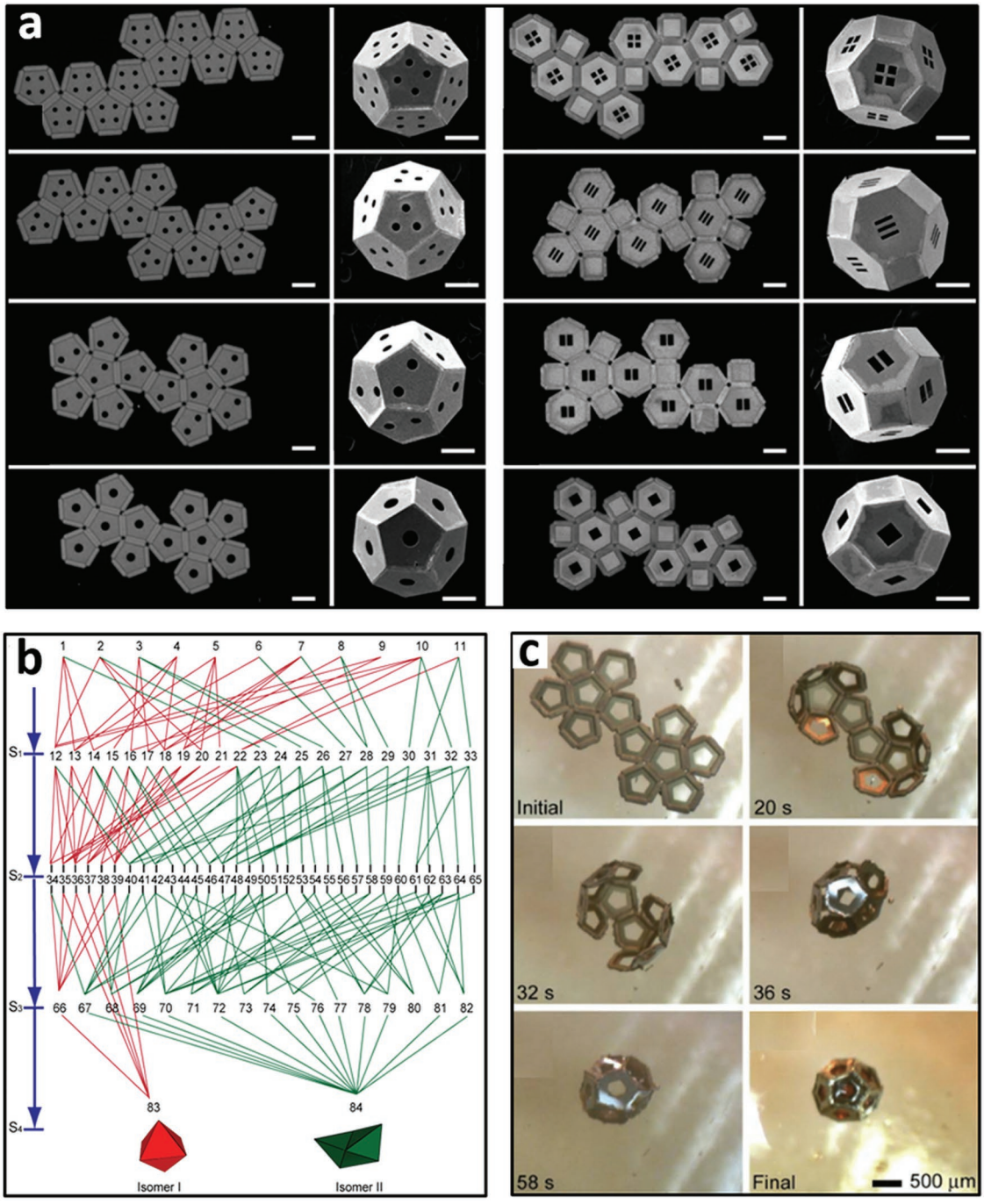

Figure 5. Geometric design considerations and assembly pathways of capillary self-folding polyhedra with hingeless capillary locking. a) SEM images of self-folding of dodecahedra and truncated octahedra with precursor 2D nets with different radii of gyration (R_g) and different numbers of vertex connections (V_c). Nets with smaller R_g and larger V_c assemble with higher yields. Scale bar indicates 300 µm. Reproduced with permission.[93] Copyright 2011, National Academy of Sciences. b) Pathways during self-folding of two octahedral isomers from the same precursor nets, illustrating that self-folding of each isomer involves different pathways. Adapted under the terms of a Creative Commons Attribution 4.0 International License.[115] Copyright 2014, The Authors, published by PLOS. c) Video snapshots featuring the hierarchical capillary force drive self-folding of a 500 µm dodecahedron. Reproduced with permission.[109] Copyright 2009, IOP Publishing.

of gyration (R_g) and with nets featuring high secondary neighbors or vertex connections (secondary panels are those not directly connected by a folding hinge but that can interact with an aligning hinge).[93,115] For instance, for defect-free capillary self-folding of truncated octahedra, Pandey et al. observed significantly higher yields of ≈30% for nets with R_g = 853 versus 16% for nets with R_g = 912 µm (**Figure 5**a).[93] Interestingly, and despite the huge combinatorial space, dominant pathways

and intermediates were observed in the self-folding process of polyhedra (Figure 5b).[115] Importantly, intermediates that were more rigid with fewer degrees of freedom were preferred. Collectively, the unraveling of such rules greatly aids the problem of inverse design of complex structures by self-folding.[115,116] The optimal use of nearest neighbors and compact nets can enable defect tolerance and error correction.[109] As shown by the snapshots during self-folding (Figure 5c), the intermediate state at 36 s appears defective, but the defect self-corrects in the subsequent steps and a perfect polyhedron is formed at the final stage.

To summarize, the design rules discovered for capillary assisted self-assembly of polyhedra using folding and aligning hinges include: a) the design of compact nets with low radii of gyration, b) the use of nets with high secondary panels, and c) the design of pathways that feature intermediates that are rigid with low degrees of freedom.

5. Applications

Capillary self-folding devices open up new applications in micro- and nano-technology, by providing precisely assembled 3D structures with the precision of 2D planar lithography. Specifically, capillary forces have allowed assembly of patterned tubes, sphere-like geometries, and polyhedra with precise 3D patterns that are challenging to fabricate by alternative methods. We highlight a few application areas and notable examples below.

5.1. Energy Harvesting

Silicon based solar cells are a major clean energy solution to reduce carbon emissions. However, as compared to spherical geometries, flat silicon solar cells have reduced light trapping ability, and typically a fixed spatial orientation whereas the sun moves constantly relative to it. It is estimated that single-crystal silicon needs to absorb more than 90% of light in order to achieve optimal efficiency.[138,139] Self-folding of light absorbing and energy harvesting devices provides a means to realize 3D geometries that can trap more light over a range of different irradiation angles as compared to planar geometries. Guo et al. assembled a 3D Si-based solar cell using capillary forces associated with drying of a water droplet placed at the center of flat panels (**Figure 6**a).[89] Importantly, the self-folding strategy leveraged well-established planar technologies; consequently their 3D cells featured single-crystal silicon with high carrier mobility and lithographically patterned photovoltaic devices. This 3D photovoltaic device self-assembled using capillary forces showed improved performance as compared to its planar precursor. The short circuit current and open circuit voltage of the cylindrical solar cell were about five- and three-fold respectively as compared to the flat solar cell. This demonstration highlights a significant advantage of self-folding as compared to other 3D fabrication strategies such as stereolithography or 3D printing which cannot create structures with high performance materials such as single-crystal silicon.

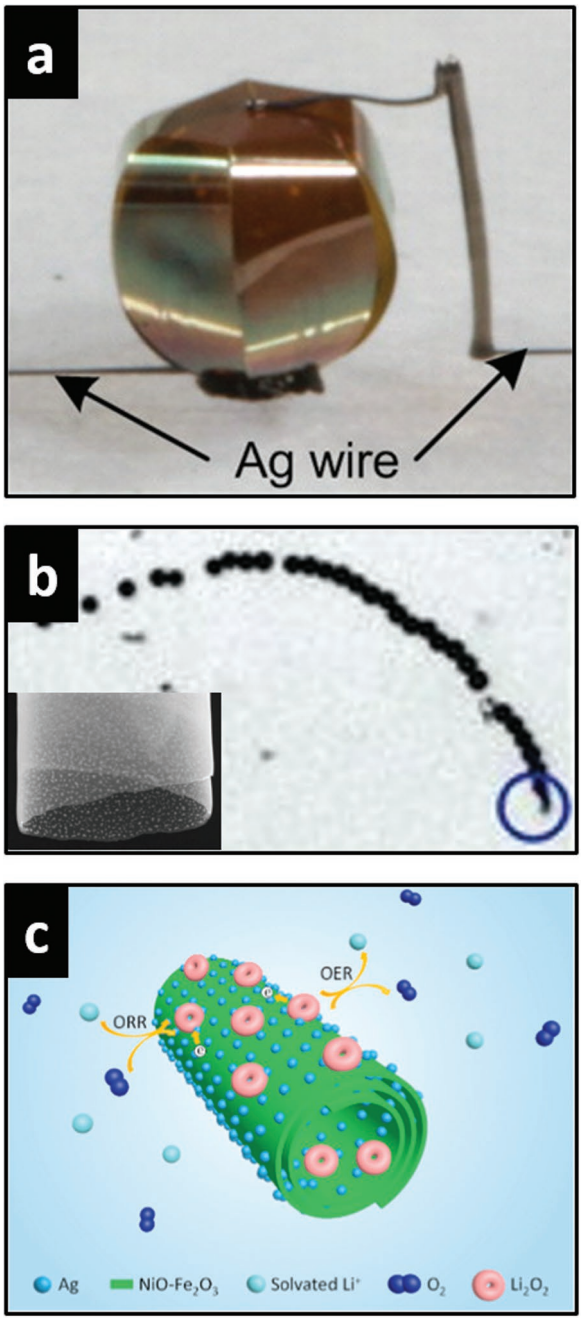

Figure 6. Capillary self-folding of energy harvesting devices. a) Optical image of a functional millimeter-sized self-folded solar cell consisting of a folded spherical single-crystal silicon shell, inner glass bead, and printed silver electrodes. Reproduced with permission.[89] Copyright 2009, National Academy of Sciences. b) Optical image of the trajectory of a catalytic SiO/SiO_2 tubular engine. Insert shows the SEM image of the rolled-up nanotube assembled using a combination of capillary and intrinsic stress forces. Reproduced with permission.[141] Copyright 2013, Wiley VCH. c) Schematic of the discharge–charge processes on the Ag/NFO/Ag electrode assembled using a combination of capillary and intrinsic stress forces. Reproduced with permission.[144] Copyright 2019, Elsevier.

Catalytic nanoengines are devices that incorporate a catalyst, typically platinum, that can react with the environment, such as hydrogen peroxide, to form bubbles of gas that cause them

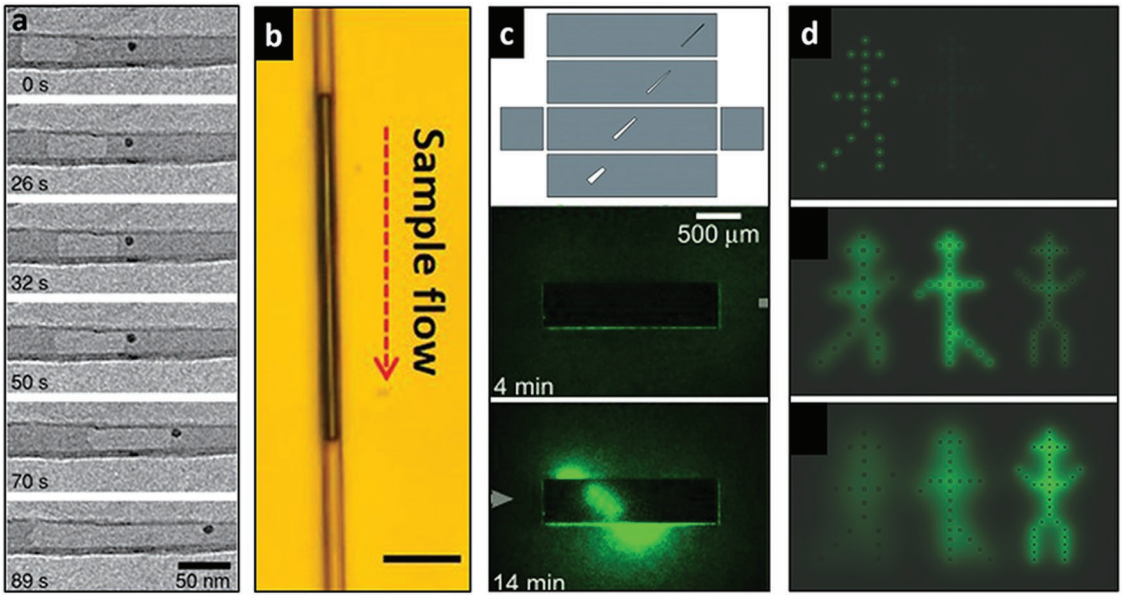

Figure 7. Capillary self-folding of micro- and nano-fluidic devices. a) TEM image showing a bubble, a 10 nm gold nanoparticle, and accompanying water column flowing from left to right in a graphene nanochannel rolled up using capillary forces. Reproduced with permission.[51] Copyright 2013, Royal Society of Chemistry. b) Optical image of small-volume pesticide solution pumped in a plasmon nanocavity self-folded using a combination of capillary forces and differential stress. Scale bar represents 3 µm. Adapted under the terms of a Creative Commons Attribution 4.0 International License.[146] Copyright 2015, The Authors, published by Springer Nature. c) Capillary self-folding of a rectangular parallelepiped-shaped container with a helical pore distribution. The top panel shows the layout of the precursor 2D net with patterned slits. The middle and bottom panel show time-lapse images of green fluorescent *E. coli* bacteria self-organizing in a helical pattern around such a container releasing a chemoattractant. Reproduced with permission.[147] Copyright 2011, Wiley VCH. d) Self-folded cubic containers with precisely engineered shape, pore size, and pattern arranged to form a chemical display that can generate an animation of a "running man" based on programmed diffusion. Reproduced with permission.[148] Copyright 2015, Wiley VCH.

to self-propel. Essentially, they harvest energy from a chemical reaction with a reactant present in the environment. Due to their untethered and autonomous nature, such nanoengines have been widely utilized in biomedical applications, chemical sensing and robotics.[140] Li et al. used rapid thermal annealing to drive dewetting of gold, silver and platinum particles on a SiO/SiO_2 film causing the assembly of nanotubes by a combination of capillary forces and stress mismatch (Figure 6b).[141] When nanotubes with Pt particles were assembled, Pt catalyzed the decomposition of hydrogen peroxide to form oxygen bubbles causing propulsion of the nanoengines. Interestingly, the dewet rough surface morphology allowed the nanoengines to move at higher speed (1630 µm s^{-1}) compared to a flat Pt film (400 µm s^{-1}).

Lithium-air (Li-O_2) batteries are a class of promising energy storage devices that can have the potential to outperform conventional Li-ion batteries. The estimated specific energy density of Li-O_2 batteries is between 500 and 900 Wh kg^{-1}, whereas that of Li-ion batteries is only about 140 Wh kg^{-1}. This would reduce the cost of the batteries by about four times.[142] One of the challenges of Li-O_2 batteries is the need to substitute the cathode with carbon-free materials, because carbon can react with Li_2O_2 and reduce the rechargeability of Li-O_2 batteries.[143] Lu et al. prepared a carbon-free cathode tube by dewetting 5 nm silver nanoparticles deposited on both sides of 30 nm-thick nickel and iron (NFO) films (Figure 6c).[144] The interplay between capillary forces and stress mismatch could be used to control the tube diameter and improve transport of the electrolyte, reactant and product. These hybrid nanomembranes showed improved mechanical and chemical stability, and Ag/NFO/Ag tubes could be cycled 180 times at 300 mA g^{-1} without significant degradation as compared to NFO and NFO/Ag, which degraded at the 53rd and 90th cycles respectively.

5.2. Micro- and Nano-Fluidics

Conventional micro- and nano-fluidic devices are fabricated by soft-lithography, molding and bonding PDMS, resulting in inherently planar geometries and channels with rectangular cross-sections. Nevertheless, channels with circular cross-section more accurately mimic biological fluidic channels and enable uniform fluid flow.[145] Capillary assembly can provide a means to roll up films and create microfluidic channels with circular cross-sections. For example, Mirsaidov et al. prepared graphene nanotubes using capillary force self-assembly of suspended graphene on grids using water (**Figure 7**a).[51] The diameter of the graphene nanotubes ranged between 20–60 nm. Apart from circular channel walls, the impervious graphene film offered the additional advantage of being able to trap liquid and air bubbles for imaging in vacuum using a transmission electron microscope (TEM). In addition, capillary assembly of tubular microfluidic structures can also increase the sensitivity of biosensors. Zhang et al. fabricated tubular nanocavities with a diameter of 850 nm by combining the stress mismatch of SiO and TiO_2 and capillary forces resulting from the melting of deposited silver nanoparticles (Figure 7b).[146] They flowed liquid samples into the tubular nanocavities, and showed ultrasensitive surface-enhanced Raman spectroscopy (SERS)-based

sensing due to the synergistic effects of surface plasmon enhancement and whispering-gallery modes. They could detect 10^{-12} M of rhodamine solution (R6G) and 10^{-5} M of the pesticide parathion, which was orders of magnitude more sensitive as compared to flat SERS substrates.

Capillary self-folded containers have also been widely utilized in creating spatiotemporal patterns of relevance to micro- and nano-fluidics. For example, Kalinin et al. spatially arranged slits on a 2D polygonal net (Figure 7c) and self-folded a rectangular parallelepiped-shaped container with a 3D helical arrangement of slits. Such containers loaded with L-serine, a bacterial chemoattractant, were placed in a chamber seeded with *Escherichia coli* bacteria expressing green fluorescent protein (GFP). Due to spatially controlled release of the chemoattractant with a 3D helical spatial profile, the *E. coli* were observed to spatially organize in a helical shape.[147] This demonstration highlights the ability of self-folding to realize containers and capsules with complex patterns of pores on all of their 3D surfaces. In addition, since the self-assembly process is highly parallel, many containers could be formed at once, such that they could be printed or arranged like voxels in a display. Kalinin et al. created such a dynamic chemical display by varying the concentration of the fluorescent dye fluorescein (Figure 7d),[148] the surface porosity, volume, shape and relative arrangement of the containers to control diffusion and realize the autonomous formation of the animation of a running man.

5.3. Drug Delivery and Cell Encapsulation Devices

Self-folded microscopic tubes and polyhedra with precisely patterned porosity can be used to create capsules with extremely precise spatio-temporal release characteristics.[149] Leong et al. showed spatiotemporal control over chemistry by loading capillary self-folded polyhedra loaded with different potassium hydroxide and phenolphthalein using stereotactic microinjection (**Figure 8**a).[150] The reaction occurred at the interface between chemicals diffusing from two containers and could be spatially controlled such that either isotropic or anisotropic chemical reactions and patterns could be formed. Such spatially controlled chemical release by 3D pore size and spatial position is important for drug delivery applications that require spatially directed release, such as in nerve regeneration.[151] Likewise, Ye et al. utilized radio-frequency (RF) electromagnetic fields to heat up capillary self-folding metallic containers to realize remotely controlled chemical release to live mouse fibroblast cells (Figure 8b).[152,153]

Self-folding polyhedra can also function as nano- or microporous capsules for cell encapsulation therapy (CET). CET is a therapeutic strategy to replace damaged or diseased cells such as pancreatic islets with foreign cells. To minimize attack from immune cells it is necessary to encapsulate the cells in precisely engineered size-exclusion membranes that can block larger immune components while permitting passage of smaller therapeutic or essential molecules such as insulin and oxygen. Also, since large numbers of cells are needed for therapies such as for treatment of Type 1 diabetes, efficient diffusion of oxygen also becomes critical to enhance cell viability and minimize necrotic zones.[154–157] Randall et al. showed that the cell viability of pancreatic β-cells in the five porous faced arrays of microwells formed by capillary self-folding is significantly higher than the one porous face arrays (Figure 8c).[158] The concentration of the released insulin from five porous faced microwell arrays was 2.20 ± 0.14 ng mL^{-1} and no insulin was detected from the 2D microwell arrays after 28 days. The authors hypothesized that diffusion in the 2D microwell was limited as compared to the 3D porous faced microwells. The simulation of cell viability in 2D and 3D porous microwells showed a 50% difference due to the limited O_2 reaching the β-cells in the 2D microwell. In addition, Azam et al. designed more biofriendly self-folded polymeric containers with SU-8 panels and biodegradable polycaprolactone (PCL) hinges wherein self-folding occurred at a lower temperature due to the lower melting point of PCL (Figure 8d).[159] The polymeric containers were also optically transparent, which allowed optical monitoring and imaging of *E. coli* culture and good cell viability. Since the containers can be mass produced, they could also be used to assemble bioartificial "organ-like" geometries such as a bioartificial pancreas[160] as well as arrayed immunoisolation devices.[158]

5.4. Electromagnetic Devices

At the macroscale, electromagnetic devices often have elaborate 3D geometries such as horn, dish, spiral, and helical antennas. These geometries can be challenging to fabricate at small size scales due to the inherent planarity of micro- and nano-lithography. Capillary self-folding can be used to transform planar electromagnetic devices into 3D geometries, as first illustrated by Dahlmann et al (**Figure 9**a).[161] They rotated an electroplated copper microwave inductor by melting lead/tin solder hinges. The 3D inductor was about 0.1 mm^2 and the quality factor of the self-folded inductor increased by ≈2.5 times as compared to the flat inductor at 1 GHz. Capillary self-folding with multiple panels can also be used to assemble electromagnetic devices and antennas that are omnidirectional and enable sensing or detection with angular information.[162–165] For example, by patterning functional sensing elements on all faces of a cube, it was possible to sense chemicals deposited at multiple angles.[166,167] One of the challenges in the miniaturization of wireless electronic devices is to minimize the size of antennas without compromising the radiation efficiency for applications such as in bioimplants or smart dust. The problem is especially urgent for electrically small antennas, i.e., antennas where the physical size is much smaller than the wavelength of the signal. Anacleto et al. demonstrated wireless energy transfer to electrically small self-folded 500 μm^3 cubic antennas in dispersive media (Figure 9b).[168] The results indicated the self-folded 3D antenna was ≈10 times more efficient at transferring energy from a RF signal as compared to the 2D unfolded flat antenna. The maximum of the scattering parameter S_{21}, which indicates power transmission efficiency for the 3D antenna was −18.3 dB at 3.6 GHz as compared to −28.6 dB at 4.8 GHz for the 2D antenna. Importantly, the self-folded cubic antenna was able to wirelessly harvest enough power (30 mW) to power a light emitting diode (LED) from a primary energy source at a distance of several centimeters.

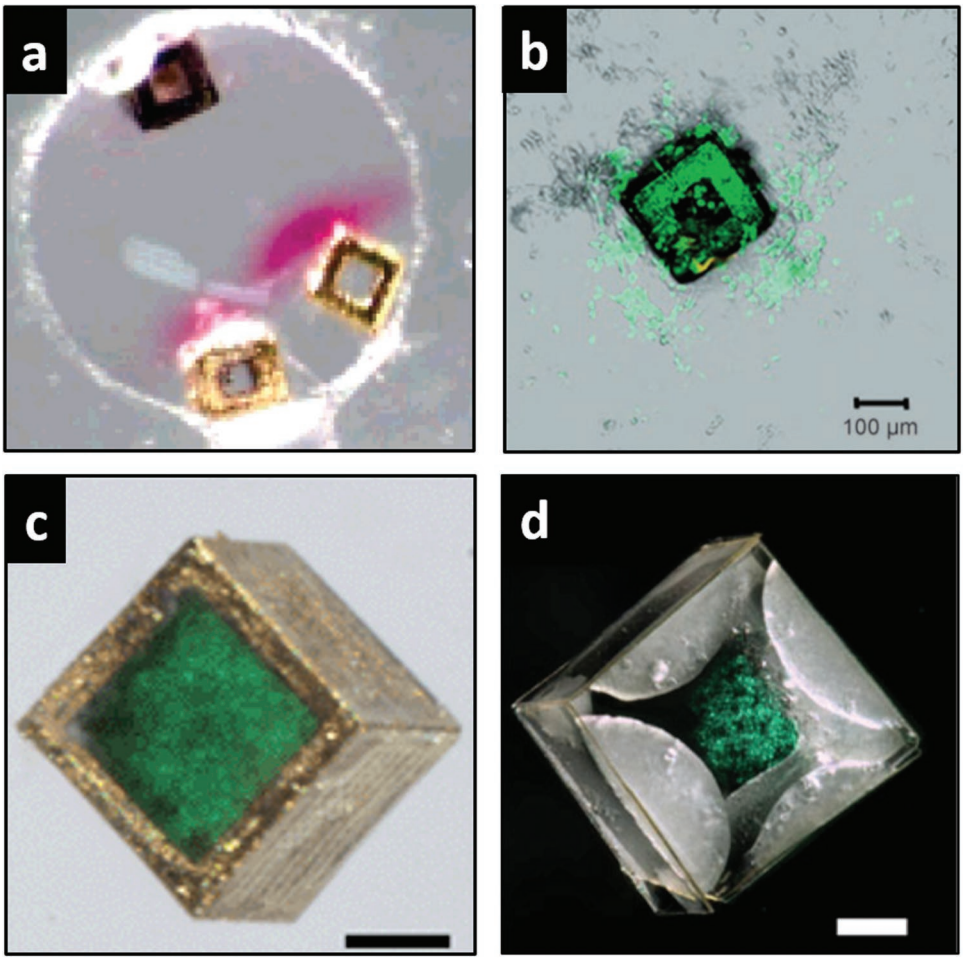

Figure 8. Capillary self-folding of drug delivery and cell encapsulation devices. a) Optical image of spatially controlled chemical reactions between multiple 100 μm sized cubic containers assembled using capillary self-folding. Reproduced with permission.[150] Copyright 2006, American Chemical Society. b) Confocal images of the local, spatially controlled release of a live/dead stain to L929 mouse fibroblast cells using a cubic container assembled using capillary self-folding. Reproduced with permission.[153] Copyright 2007, Wiley-VCH. c) Optical image of live β-TC-6 cells loaded into microwells with controlled porosity in all three dimensions and assembled using capillary self-folding. Reproduced with permission.[158] Copyright 2011, The Royal Society of Chemistry. d) Bright-field image of stained fibroblast cells encapsulated within a polymeric container assembled using capillary self-folding. Reproduced with permission.[159] Copyright 2010, Springer Nature.

Self-folding of polyhedra can also be used to create metallic structures where induced current can flow along all three dimensions, which is important to manipulate polarization of electromagnetic responses, as illustrated by Randhawa et al. for THz responsive cubes (Figure 9c).[169] Also, more complex and much smaller designs can be implemented for nanoscale optical devices. For example, Cho et al. self-folded 100 nm scale cubes with metallic (Au) single and double split-ring resonators (SRRs) on dielectric panels (aluminum oxide, Al_2O_3) (Figure 9d).[170] The SRRs align such that they are along each of the three axes, which is important for generating metamaterials with unusual optical properties when arrayed. Electromagnetic simulations additionally suggested that designs with metal features along each of the three axes could enhance quadrupolar modes, which are important for high sensitivity biosensors.

Self-folding cubes can be used as a scaffold to suspend novel atomistic materials such as graphene and graphene oxide to create novel electromagnetic devices.[171–174] Joung et al. demonstrated tunable optically transparent self-folded polyhedra with freestanding graphene oxide panels and solder hinges (Figure 9e).[171] By controlling 10–40 layers of graphene oxide, the optical transparency changed from 50% to 0% when the polyhedra were wet as opposed to completely dry. They attributed this observation to diffusion of water molecules into the layers of graphene oxide. Joung et al. also reported a method to integrate graphene in micro- and nano-scale self-folded cubes by reflowing polymer hinges (Figure 9f).[172] Specifically, SU-8 frames and SPR 220 polymer hinges were patterned on top of graphene, and the polymer could be reflowed at 100 °C, which is lower than the temperature used in solder reflow. Similarly, nanoscale cubes were assembled with Al_2O_3 panels and PMMA hinges. The simulated electric field suggested that the surface of the 3D graphene cube had approximately four times enhancement as compared to the planar graphene ribbon.

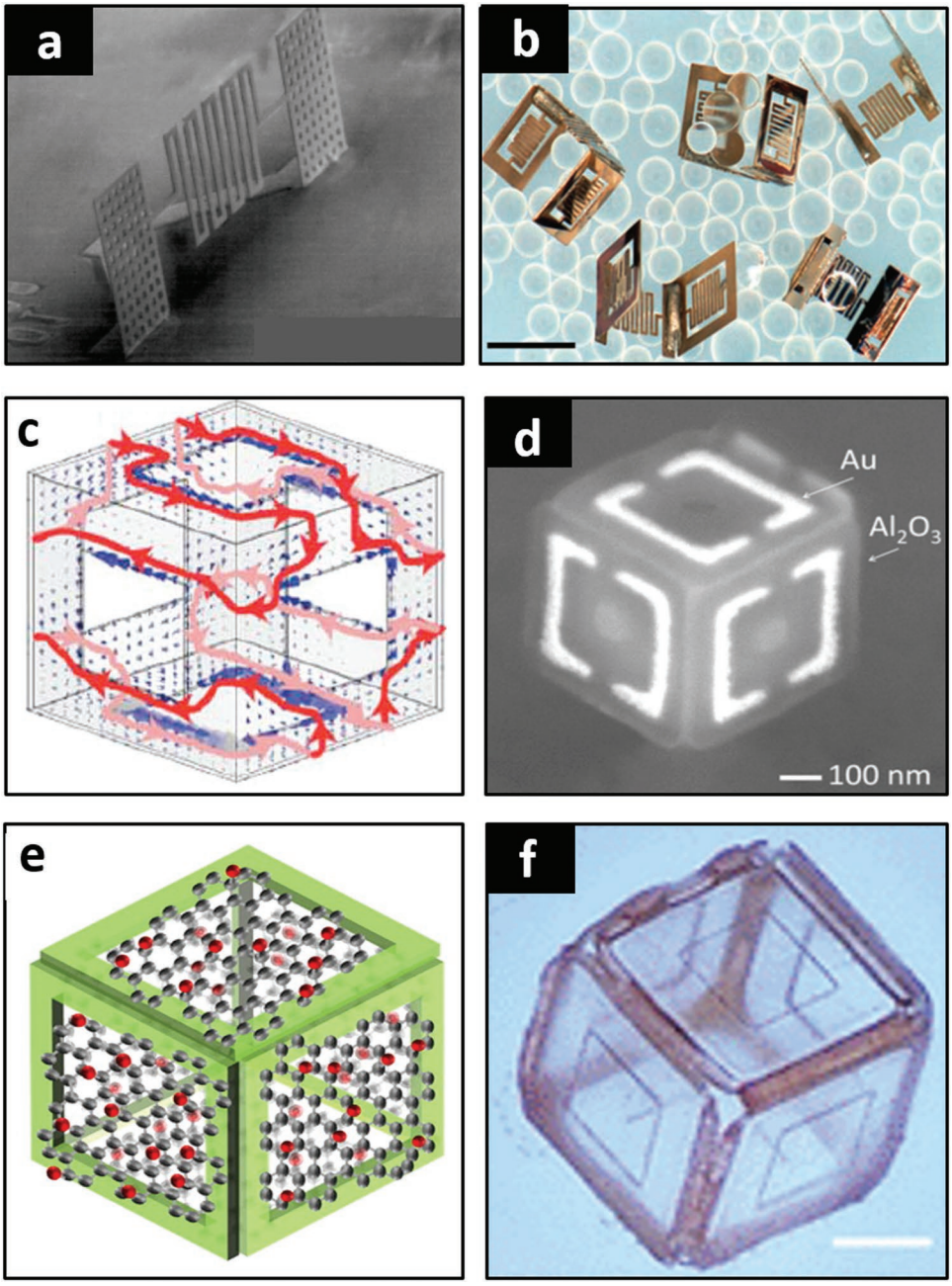

Figure 9. Capillary self-folding of electromagnetic devices. a) SEM image of an inductor structure after capillary self-folding. Reproduced with permission.[161] Copyright 2000, Institution of Engineering and Technology. b) Optical images of microcube antennas after capillary self-folding. Scale bar represents 500 µm. Reproduced with permission.[168] Copyright 2016, World Scientific Publishing Co. Inc. c) Simulated surface current density in a hollow cubic geometry illustrating that current loops can travel in all three dimensions. Reproduced with permission.[169] Copyright 2010, American Institute of Physics. d) SEM images of a capillary self-folded nanocube with Au twin loop SRRs on Al_2O_3 panels. Reproduced with permission.[170] Copyright 2011, Wiley-VCH. e) Schematic of a capillary self-folded cube with freestanding graphene oxide suspended on the frames. Reproduced with permission.[171] Copyright 2016, American Chemical Society. f) Optical image of a capillary self-folded cube with freestanding graphene on the frames. Scale bar represents 100 µm. Reproduced with permission.[172] Copyright 2017, American Chemical Society.

6. Conclusion

Capillary self-folding can be conveniently utilized to bend or rotate continuous substrates or micro-/nano-machined panels and create a range of 3D shapes such as curved tubes, sphere-like geometries, and polyhedra. The approach is straightforward and scales favorably, suggesting potentially widespread applicability in micro- and nano-manufacturing. This versatile technique is compatible with planar lithographic techniques such as photo-, e-beam,[174,175] nanoimprint,[176] and soft lithography, as well as with direct ink writing and 3D printing. Hence, for the first time now, it is conceivable that

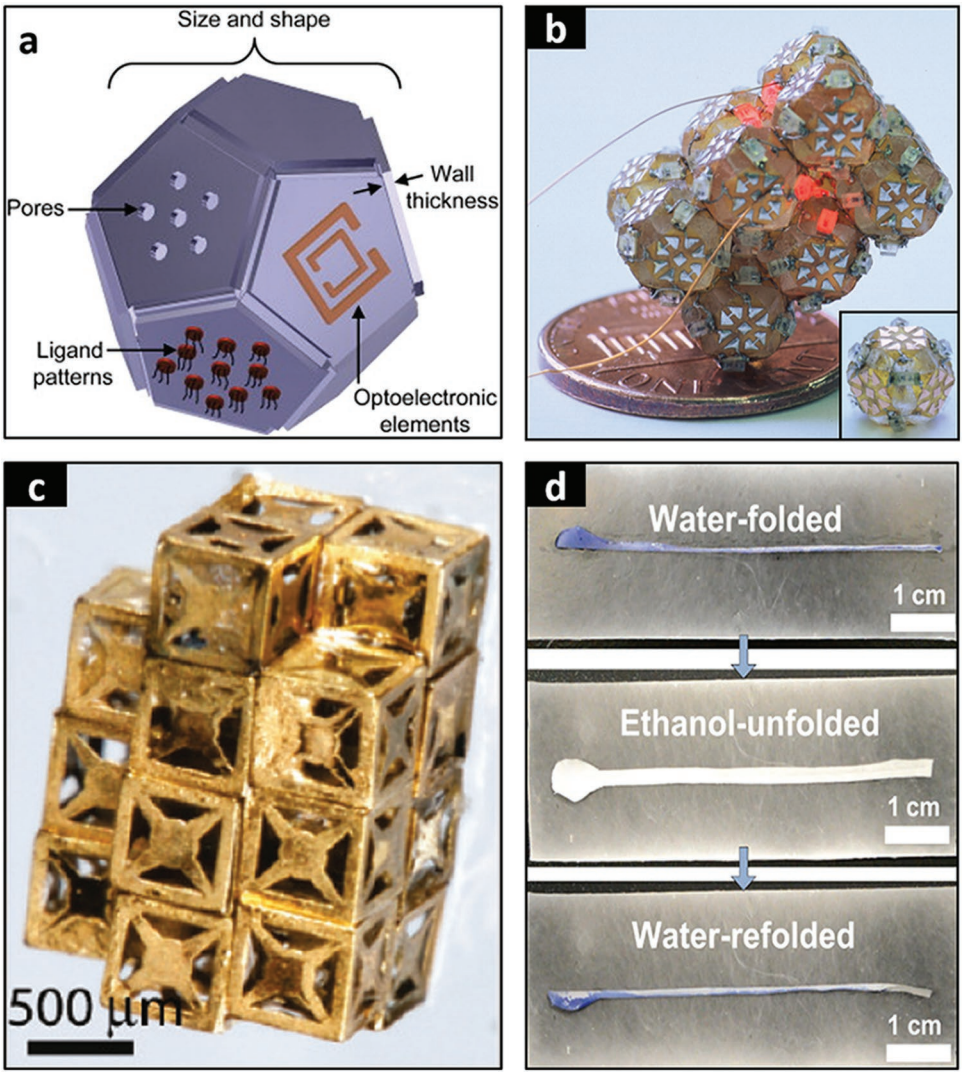

Figure 10. Outlook and Future directions. a) Conceptual schematic of a hypothetical drug release capsule with precise shape and spatial pattern of pores, electromagnetic element for sensing and communication and biomolecular ligand pattern. Reproduced with permission.[177] Copyright 2012, Elsevier. b) A 3D electrical network with serial connectivity formed by aggregated self-assembly of polyhedral building blocks with LEDs, wiring, and contact pads. Reproduced with permission.[14] Copyright 2000, American Association for the Advancement of Science. c) Optical image of self-assembled THz responsive metamaterial aggregate formed using cubic blocks self-folded using capillary forces. Reproduced with permission.[178] Copyright 2010, American Chemical Society. d) Optical images of dynamic folding and unfolding of Janus bilayers. Reproduced with permission.[125] Copyright 2016, American Association for the Advancement of Science.

extremely complex particles could be assembled with precise shape and surface patterning in a highly reproducible manner. The example in **Figure 10**a illustrates a futuristic drug delivery capsule or particle with spatially engineered porosity, electromagnetic element for potentially wireless sensing or actuation, and receptors for targeted binding.[177] Such conceivable capsules and particles would require heterogeneous integration of different material classes such as metals, semiconductors, insulators, polymers, and organic molecules. They cannot be assembled at the present time, but, as argued in this paper, they could potentially be assembled in the near future by folding precisely patterned precursors, in a process whereby the functional elements are designed into a net using well-established patterning approaches and then transformed into 3D geometries through a final capillary self-folding step. Also, capillary self-folding of polyhedra is amenable to the assembly of large numbers of particles in a single step as it occurs in a highly parallel fashion. Also, solidification of liquid hinges composed of solder or polymers on cooling allow such self-folded polyhedra to be permanently bonded and sealed in-place. Consequently, such polyhedra could be used as building blocks for aggregative assembly of 3D metamaterials (Figure 10b), 3D electrical networks, (Figure 10c) and 3D computational devices,[14,178,179] which is not presently possible by other approaches. Also, as previously mentioned, it would be interesting to manipulate surface properties or surface tension to create dynamic and reversible structures. A preliminary demonstration by Wong et al. illustrates this idea, whereby a tube composed of PCL nanofibers

and polyvinyl chloride (PVC) microfibers is folded and unfolded upon replacement of water with ethanol (Figure 10d).[125] Finally, while this review mainly discussed organized self-folding of lithographically or precisely patterned precursors, folding using bulk processes driven by capillary forces, while significantly less precise, offers the possibility for the creation of large numbers of unique 3D geometries such as crumpled nanosheets and sacks of graphene oxide.[180–187]

In summary, we envision that due to its combined advantageous attributes—which include favorable force scaling to small sizes, extreme miniaturization, compatibility with conventional lithographical patterning approaches, high-throughput assembly, and potential dynamic manipulation—capillary self-folding could significantly augment present day planar and robotic micro- and nano-manufacturing to be of high relevance to science, engineering, and medicine.

Acknowledgements

K.S.K. and Q.H. contributed equally to this work. The research reported in this publication was supported by the Air Force Office of Scientific Research MURI program (Grant No. FA9550-16-1-0031) and the National Science Foundation (Grant Nos. CMMI-1635443, DMR-1507749, and DMR-1709349). The content is solely the responsibility of the authors and does not necessarily represent the official views of the funding agencies.

Conflict of Interest

The authors declare no conflict of interest.

Keywords

elastocapillarity, micro-electromechanical systems, origami, self-assembly, surface tension

Received: September 30, 2019
Revised: November 4, 2019
Published online:

[1] M. P. Groover, *Fundamentals of Modern Manufacturing: Materials, Processes, and Systems*, John Wiley & Sons, Inc., Hoboken, NJ **2020**.
[2] S. A. Campbell, *The Science and Engineering of Microelectronic Fabrication*, Oxford University Press, New York **2011**.
[3] Y. Zhang, F. Zhang, Z. Yan, Q. Ma, X. Li, Y. Huang, J. A. Rogers, *Nat. Rev. Mater.* **2017**, *2*, 17019.
[4] G. Huang, Y. Mei, *Small* **2018**, *14*, 1703665.
[5] K. Agarwal, S. Hwang, A. Bartnik, N. Buchele, A. Mishra, J.-H. Cho, *Small* **2018**, *14*, 1801145.
[6] Z. Liu, A. Cui, J. Li, C. Gu, *Adv. Mater.* **2019**, *31*, 1802211.
[7] N. Lazarus, G. L. Smith, M. D. Dickey, *Adv. Intell. Syst.* **2019**, *1*, 1900059.
[8] D. Karnaushenko, T. Kang, V. K. Bandari, F. Zhu, O. G. Schmidt, *Adv. Mater.* **2019**, 1902994.
[9] M. Gauthier, S. Régnier, *Robotic Microassembly*, John Wiley & Sons, Inc., Hoboken, NJ **2010**.
[10] M. Mastrangeli, S. Abbasi, C. Varel, C. Van Hoof, J.-P. Celis, K. F. Böhringer, *J. Micromech. Microeng.* **2009**, *19*, 083001.
[11] G. M. Whitesides, B. Grzybowski, *Science* **2002**, *295*, 2418.
[12] J. Lehn, *Science* **1993**, *260*, 1762.
[13] C. A. Mirkin, R. L. Letsinger, R. C. Mucic, J. J. Storhoff, *Nature* **1996**, *382*, 607.
[14] D. H. Gracias, J. Tien, T. L. Breen, C. Hsu, G. M. Whitesides, *Science* **2000**, *289*, 1170.
[15] M. Boncheva, G. M. Whitesides, *MRS Bull.* **2005**, *30*, 736.
[16] R. Groß, M. Dorigo, *Proc. IEEE* **2008**, *96*, 1490.
[17] Y. Mei, G. Huang, A. A. Solovev, E. B. Ureña, I. Mönch, F. Ding, T. Reindl, R. K. Y. Fu, P. K. Chu, O. G. Schmidt, *Adv. Mater.* **2008**, *20*, 4085.
[18] L. Ionov, *Soft Matter* **2011**, *7*, 6786.
[19] Y. Mei, A. A. Solovev, S. Sanchez, O. G. Schmidt, *Chem. Soc. Rev.* **2011**, *40*, 2109.
[20] E. A. Peraza-Hernandez, D. J. Hartl, R. J. Malak Jr., D. C. Lagoudas, *Smart Mater. Struct.* **2014**, *23*, 094001.
[21] Y. Liu, J. Genzer, M. D. Dickey, *Prog. Polym. Sci.* **2016**, *52*, 79.
[22] J. Rogers, Y. Huang, O. G. Schmidt, D. H. Gracias, *MRS Bull.* **2016**, *41*, 123.
[23] V. A. Bolaños Quiñones, H. Zhu, A. A. Solovev, Y. Mei, D. H. Gracias, *Adv. Biosyst.* **2018**, *2*, 1800230.
[24] P.-G. de Gennes, F. Brochard-Wyart, D. Quéré, *Capillarity and Wetting Phenomena*, Springer, New York **2004**.
[25] R. Hensel, C. Neinhuis, C. Werner, *Chem. Soc. Rev.* **2016**, *45*, 323.
[26] B. Bhushan, E. K. Her, *Langmuir* **2010**, *26*, 8207.
[27] D. H. Trevena, *J. Phys: D. Appl. Phys.* **1984**, *17*, 2139.
[28] M. T. Tyree, M. H. Zimmermann, *Xylem Structure and the Ascent of Sap*, 1st ed., Springer, Berlin **2002**.
[29] J. Ju, H. Bai, Y. Zheng, T. Zhao, R. Fang, L. Jiang, *Nat. Commun.* **2012**, *3*, 1247.
[30] M. T. Tyree, M. H. Zimmermann, *Xylem Structure and the Ascent of Sap*, 1st ed., Springer, Berlin **2002**, pp. 49–88.
[31] J. E. Armstrong, *Am. J. Bot.* **2002**, *89*, 362.
[32] M. Prakash, D. Quéré, J. W. M. Bush, *Science* **2008**, *320*, 931.
[33] A. Rico-Guevara, M. A. Rubega, *Proc. Natl. Acad. Sci. USA* **2011**, *108*, 9356.
[34] A. Rico-Guevara, T.-H. Fan, M. A. Rubega, *Proc. R. Soc. B* **2015**, *282*, 20151014.
[35] C. Duprat, S. Protière, A. Y. Beebe, H. A. Stone, *Nature* **2012**, *482*, 510.
[36] W. Federle, W. J. P. Barnes, W. Baumgartner, P. Drechsler, J. M. Smith, *J. R. Soc., Interface* **2006**, *3*, 689.
[37] S. Gernay, W. Federle, P. Lambert, T. Gilet, *J. R. Soc., Interface* **2016**, *13*, 20160371.
[38] J. S. Koh, E. Yang, G. P. Jung, S. P. Jung, J. H. Son, S. I. Lee, P. G. Jablonski, R. J. Wood, H. Y. Kim, K. J. Cho, *Science* **2015**, *349*, 517.
[39] D. L. Hu, J. W. M. Bush, *Nature* **2005**, *437*, 733.
[40] J. W. M. Bush, D. L. Hu, M. Prakash, *Adv. Insect Physiol.* **2007**, *34*, 117.
[41] D. L. Hu, J. W. M. Bush, *J. Fluid Mech.* **2010**, *644*, 5.
[42] M. R. Flynn, J. W. M. Bush, *J. Fluid Mech.* **2008**, *608*, 275.
[43] F. Vollrath, D. T. Edmonds, *Nature* **1989**, *340*, 305.
[44] H. Elettro, S. Neukirch, F. Vollrath, A. Antkowiak, *Proc. Natl. Acad. Sci. USA* **2016**, *113*, 6143.
[45] J. B. Grotberg, O. E. Jensen, *Annu. Rev. Fluid Mech.* **2004**, *36*, 121.
[46] M. Heil, A. L. Hazel, J. A. Smith, *Respir. Physiol. Neurobiol.* **2008**, *163*, 214.
[47] M. Heil, A. L. Hazel, in *Fluid-Structure Interactions in Low-Reynolds-Number Flows* (Eds: C. Duprat, H. A. Stone), The Royal Society of Chemistry, Cambridge **2016**, pp. 280–312.
[48] D. Gonzalez-Rodriguez, S. Sart, A. Babataheri, D. Tareste, A. I. Barakat, C. Clanet, J. Husson, *Phys. Rev. Lett.* **2015**, *115*, 088102.
[49] P. Lambert, M. Mastrangeli, *Microscale Surface Tension and Its Applications*, MDPI AG, Basel **2019**.
[50] T. G. Leong, A. M. Zarafshar, D. H. Gracias, *Small* **2010**, *6*, 792.

[51] U. Mirsaidov, V. R. S. S. Mokkapati, D. Bhattacharya, H. Andersen, M. Bosman, B. Özyilmaz, P. Matsudaira, *Lab Chip* **2013**, *13*, 2874.
[52] J. Bae, T. Ouchi, R. C. Hayward, *ACS Appl. Mater. Interfaces* **2015**, *7*, 14734.
[53] M. Li, Q. Yang, H. Liu, M. Qiu, T. J. Lu, F. Xu, *Small* **2016**, *12*, 4492.
[54] M. F. Reynolds, K. L. McGill, M. A. Wang, H. Gao, F. Mujid, K. Kang, J. Park, M. Z. Miskin, I. Cohen, P. L. McEuen, *Nano Lett.* **2019**, *19*, 6221.
[55] J.-B. Valsamis, M. De Volder, P. Lambert, in *Surface Tension In Microsystems Engineering Below the Capillary Length* (Eds: P. Lambert), Springer, Berlin **2013**, pp. 3–16.
[56] J. S. Rowlinson, B. Widom, *Molecular Theory of Capillarity*, Dover Publications, Mineola, NY **2003**.
[57] R. Shuttleworth, *Proc. Phys. Soc., London, Sect. A* **1950**, *63*, 444.
[58] B. Andreotti, J. H. Snoeijer, *EPL = Europhysics Letters* **2016**, *113*, 66001.
[59] J. Bico, É. Reyssat, B. Roman, *Annu. Rev. Fluid Mech.* **2018**, *50*, 629.
[60] J. Bico, B. Roman, L. Moulin, A. Boudaoud, *Nature* **2004**, *432*, 690.
[61] M. Mastrangeli, Q. Zhou, V. Sariola, P. Lambert, *Soft Matter* **2017**, *13*, 304.
[62] N. Chakrapani, B. Wei, A. Carrillo, P. M. Ajayan, R. S. Kane, *Proc. Natl. Acad. Sci. USA* **2004**, *101*, 4009.
[63] M. De Volder, A. J. Hart, *Angew. Chem., Int. Ed.* **2013**, *52*, 2412.
[64] S. H. Tawfick, J. Bico, S. Barcelo, *MRS Bull.* **2016**, *41*, 108.
[65] C. H. Mastrangelo, C. H. Hsu, *J. Microelectromech. Syst.* **1993**, *2*, 33.
[66] T. Tanaka, M. Morigami, N. Atoda, *Jpn. J. Appl. Phys.* **1993**, *32*, 6059.
[67] O. Raccurt, F. Tardif, F. A. D'Avitaya, T. Vareine, *J. Micromech. Microeng.* **2004**, *14*, 1083.
[68] M. J. Madou, *Fundamentals of Microfabrication*, CRC Press, Boca Raton, FL **2002**.
[69] K. Liu, M. Vuckovac, M. Latikka, T. Huhtamäki, R. H. A. Ras, *Science* **2019**, *363*, 1147.
[70] D. J. Donahue, F. E. Bartell, *J. Phys. Chem.* **1952**, *56*, 480.
[71] A. W. Adamson, A. P. Gast, *Physical Chemistry of Surfaces*, John Wiley & Sons, Inc., Hoboken, NJ **1997**.
[72] R. R. A. Syms, E. M. Yeatman, V. M. Bright, G. M. Whitesides, *J. Microelectromech. Syst.* **2003**, *12*, 387.
[73] A. A. Nepomnyashchy, M. G. Velarde, P. Colinet, *Interfacial Phenomena and Convection*, Chapman And Hall/CRC, Boca Raton, FL **2001**.
[74] P. Colinet, J. C. Legros, M. G. Velarde, *Nonlinear Dynamics of Surface-Tension-Driven Instabilities*, John Wiley & Sons, Inc., Hoboken, NJ **2001**.
[75] S. J. Park, B. M. Weon, J. S. Lee, J. Lee, J. Kim, J. H. Je, *Nat. Commun.* **2014**, *5*, 4369.
[76] J. D. Paulsen, V. Démery, C. D. Santangelo, T. P. Russell, B. Davidovitch, N. Menon, *Nat. Mater.* **2015**, *14*, 1206.
[77] D. Kumar, J. D. Paulsen, T. P. Russell, N. Menon, *Science* **2018**, *359*, 775.
[78] C. Py, P. Reverdy, L. Doppler, J. Bico, B. Roman, C. N. Baroud, *Phys. Rev. Lett.* **2007**, *98*, 156103.
[79] R. R. A. Syms, E. M. Yeatman, *Electron. Lett.* **1993**, *29*, 662.
[80] E. de Langre, C. N. Baroud, P. Reverdy, *J. Fluids and Struct.* **2010**, *26*, 205.
[81] S. Neukirch, A. Antkowiak, J. J. Marigo, *Proc. R. Soc. A* **2013**, *469*, 20130066.
[82] A. Antkowiak, B. Audoly, C. Josserand, S. Neukirch, M. Rivetti, *Proc. Natl. Acad. Sci. USA* **2011**, *108*, 10400.
[83] T. Jamin, C. Py, E. Falcon, *Phys. Rev. Lett.* **2011**, *107*, 204503.
[84] L. Gao, T. J. McCarthy, *Langmuir* **2008**, *24*, 9183.
[85] G. McHale, *Langmuir* **2009**, *25*, 7185.
[86] G. McHale, M. I. Newton, N. J. Shirtcliffe, N. R. Geraldi, *Beilstein J. Nanotechnol.* **2011**, *2*, 145.
[87] N. R. Geraldi, F. F. Ouali, R. H. Morris, G. McHale, M. I. Newton, *Appl. Phys. Lett.* **2013**, *102*, 214104.
[88] X. Ning, X. Wang, Y. Zhang, X. Yu, D. Choi, N. Zheng, D. S. Kim, Y. Huang, Y. Zhang, J. A. Rogers, *Adv. Mater. Interfaces* **2018**, *5*, 1800284.
[89] X. Guo, H. Li, B. Yeop Ahn, E. B. Duoss, K. J. Hsia, J. A. Lewis, R. G. Nuzzo, *Proc. Natl. Acad. Sci. USA* **2009**, *106*, 20149.
[90] S. Manakasettharn, J. Ashley Taylor, T. N. Krupenkin, *Appl. Phys. Lett.* **2011**, *99*, 144102.
[91] Z. Ren, W. Hu, X. Dong, M. Sitti, *Nat. Commun.* **2019**, *10*, 2703.
[92] J. W. Van Honschoten, J. W. Berenschot, T. Ondarçuhu, R. G. P. Sanders, J. Sundaram, M. Elwenspoek, N. R. Tas, *Appl. Phys. Lett.* **2010**, *97*, 014103.
[93] S. Pandey, M. Ewing, A. Kunas, N. Nguyen, D. H. Gracias, G. Menon, *Proc. Natl. Acad. Sci. USA* **2011**, *108*, 19885.
[94] R. Gagler, A. Bugacov, B. E. Koel, P. M. Will, *J. Micromech. Microeng.* **2008**, *18*, 055025.
[95] A. Legrain, T. G. Janson, J. W. Berenschot, L. Abelmann, N. R. Tas, *J. Appl. Phys.* **2014**, *115*, 214905.
[96] A. Legrain, E. J. W. Berenschot, N. R. Tas, A. Leon, *PLoS One* **2015**, *10*, e0125891.
[97] D. H. Gracias, V. Kavthekar, J. C. Love, K. E. Paul, G. M. Whitesides, *Adv. Mater.* **2002**, *14*, 235.
[98] R. R. A. Syms, *Sens. Actuators, A* **1998**, *65*, 238.
[99] R. R. A. Syms, *J. Microelectromech. Syst.* **1999**, *8*, 448.
[100] R. R. A. Syms, *J. Microelectromech. Syst.* **1995**, *4*, 177.
[101] K. A. Brakke, *Exp. Math.* **1992**, *1*, 141.
[102] K. F. Harsh, V. M. Bright, Y. C. Lee, *Sens. Actuators, A* **1999**, *77*, 237.
[103] T. G. Leong, P. A. Lester, T. L. Koh, E. K. Call, D. H. Gracias, *Langmuir* **2007**, *23*, 8747.
[104] K. F. Harsh, V. M. Bright, Y. C. Lee, in *50th Electronic Components & Technology Conf.*, IEEE, Las Vegas, NV **2000**, p. 1690.
[105] Y. Martin, S. Kamlapurkar, N. Marchack, J.-W. Nah, T. Barwicz, in *69th Electronic Components and Technology Conf. (ECTC)*, IEEE, Las Vegas, NV **2019**, p. 528.
[106] R. R. A. Syms, C. Gormley, S. Blackstone, *Sens. Actuators, A* **2001**, *88*, 273.
[107] E. E. Hui, R. T. Howe, M. S. Rodgers, in *Thirteenth Annual International Conf. on Micro Electro Mechanical Syst. (Cat. No.00CH36308)*, IEEE, Miyazaki, Japan **2000**, p. 602.
[108] Y. K. Hong, R. R. A. Syms, *Sens. Actuators, A* **2006**, *127*, 381.
[109] D. J. Filipiak, A. Azam, T. G. Leong, D. H. Gracias, *J. Micromech. Microeng.* **2009**, *19*, 075012.
[110] T. L. Breen, J. Tien, S. R. J. Oliver, T. Hadzic, G. M. Whitesides, *Science* **1999**, *284*, 948.
[111] L. F. Miller, *IBM J. Res. Dev.* **2000**, *44*, 93.
[112] M. J. Wale, C. Edge, *IEEE Trans. Compon., Hybrids, Manuf. Technol.* **1990**, *13*, 780.
[113] K. Sato, K. Ito, S. Hata, A. Shimokohbe, *Precis. Eng.* **2003**, *27*, 42.
[114] A. Azam, T. G. Leong, A. M. Zarafshar, D. H. Gracias, *PLoS One* **2009**, *4*, e4451.
[115] S. Pandey, D. Johnson, R. Kaplan, J. Klobusicky, G. Menon, D. H. Gracias, *PLoS One* **2014**, *9*, e108960.
[116] R. Kaplan, J. Klobušický, S. Pandey, D. H. Gracias, G. Menon, *Artif. Life* **2014**, *20*, 409.
[117] M. Behl, K. Kratz, J. Zotzmann, U. Nöchel, A. Lendlein, *Adv. Mater.* **2013**, *25*, 4466.
[118] M. Piñeirua, J. Bico, B. Roman, *Soft Matter* **2010**, *6*, 4491.
[119] J. Mu, C. Hou, H. Wang, Y. Li, Q. Zhang, M. Zhu, *Sci. Adv.* **2015**, *1*, e1500533.
[120] C. Zhang, J.-W. Su, H. Deng, Y. Xie, Z. Yan, J. Lin, *ACS Appl. Mater. Interfaces* **2017**, *9*, 41505.
[121] J. S. Randhawa, M. D. Keung, P. Tyagi, D. H. Gracias, *Adv. Mater.* **2010**, *22*, 407.

[122] J.-H. Na, A. A. Evans, J. Bae, M. C. Chiappelli, C. D. Santangelo, R. J. Lang, T. C. Hull, R. C. Hayward, *Adv. Mater.* **2015**, *27*, 79.
[123] C. Yoon, R. Xiao, J. Park, J. Cha, T. D. Nguyen, D. H. Gracias, *Smart Mater. Struct.* **2014**, *23*, 094008.
[124] J. C. Breger, C. Yoon, R. Xiao, H. R. Kwag, M. O. Wang, J. P. Fisher, T. D. Nguyen, D. H. Gracias, *ACS Appl. Mater. Interfaces* **2015**, *7*, 3398.
[125] W. S. Y. Wong, M. Li, D. R. Nisbet, V. S. J. Craig, Z. Wang, A. Tricoli, *Sci. Adv.* **2016**, *2*, e1600417.
[126] M. R. Khan, C. B. Eaker, E. F. Bowden, M. D. Dickey, *Proc. Natl. Acad. Sci. USA* **2014**, *111*, 14047.
[127] Y. Liu, P. G. Jessop, M. Cunningham, C. A. Eckert, C. L. Liotta, *Science* **2006**, *313*, 958.
[128] P. Brown, A. Bushmelev, C. P. Butts, J. Cheng, J. Eastoe, I. Grillo, R. K. Heenan, A. M. Schmidt, *Angew. Chem., Int. Ed.* **2012**, *51*, 2414.
[129] M. Cui, T. Emrick, T. P. Russell, *Science* **2013**, *342*, 460.
[130] L. D. Zarzar, V. Sresht, E. M. Sletten, J. A. Kalow, D. Blankschtein, T. M. Swager, *Nature* **2015**, *518*, 520.
[131] Z. Yang, J. Wei, Y. I. Sobolev, B. A. Grzybowski, *Nature* **2018**, *553*, 313.
[132] H. Li, X. Guo, R. G. Nuzzo, K. J. Hsia, *J. Mech. Phys. Solids* **2010**, *58*, 2033.
[133] J.-H. Cho, A. Azam, D. H. Gracias, *Langmuir* **2010**, *26*, 16534.
[134] J.-H. Cho, T. James, D. H. Gracias, *Proc. SPIE 7767, Instrumentation, Metrology, and Standards for Nanomanufacturing IV*, SPIE, Bellingham, WA **2010**, p. 776704.
[135] J.-H. Cho, D. Datta, S.-Y. Park, V. B. Shenoy, D. H. Gracias, *Nano Lett.* **2010**, *10*, 5098.
[136] J.-H. Cho, T. James, D. H. Gracias, *Adv. Mater.* **2010**, *22*, 2320.
[137] C. Dai, D. Joung, J.-H. Cho, *Nano-Micro Lett.* **2017**, *9*, 27.
[138] L. Tsakalakos, *Mater. Sci. Eng., R* **2008**, *62*, 175.
[139] M. D. Kelzenberg, S. W. Boettcher, J. A. Petykiewicz, D. B. Turner-Evans, M. C. Putnam, E. L. Warren, J. M. Spurgeon, R. M. Briggs, N. S. Lewis, H. A. Atwater, *Nat. Mater.* **2010**, *9*, 239.
[140] F. Wong, K. K. Dey, A. Sen, *Annu. Rev. Mater. Res.* **2016**, *46*, 407.
[141] J. Li, J. Zhang, W. Gao, G. Huang, Z. Di, R. Liu, J. Wang, Y. Mei, *Adv. Mater.* **2013**, *25*, 3715.
[142] P. G. Bruce, S. A. Freunberger, L. J. Hardwick, J. M. Tarascon, *Nat. Mater.* **2012**, *11*, 19.
[143] B. D. McCloskey, A. Speidel, R. Scheffler, D. C. Miller, V. Viswanathan, J. S. Hummelshøj, J. K. Nørskov, A. C. Luntz, *J. Phys. Chem. Lett.* **2012**, *3*, 997.
[144] X. Lu, Y. Yin, L. Zhang, S. Huang, L. Xi, L. Liu, S. Oswald, O. G. Schmidt, *Energy Storage Mater.* **2019**, *16*, 155.
[145] R. A. Samy, A. K. Sen, *J. Micromech. Microeng.* **2019**, *29*, 065001.
[146] J. Zhang, J. Li, S. Tang, Y. Fang, J. Wang, G. Huang, R. Liu, L. Zheng, X. Cui, Y. Mei, *Sci. Rep.* **2015**, *5*, 15012.
[147] Y. V. Kalinin, J. S. Randhawa, D. H. Gracias, *Angew. Chem., Int. Ed.* **2011**, *50*, 2549.
[148] Y. V. Kalinin, S. Pandey, J. Hong, D. H. Gracias, *Adv. Funct. Mater.* **2015**, *25*, 3998.
[149] Y. V. Kalinin, A. Murali, D. H. Gracias, *RSC Adv.* **2012**, *2*, 9707.
[150] T. Leong, Z. Gu, T. Koh, D. H. Gracias, *J. Am. Chem. Soc.* **2006**, *128*, 11336.
[151] R. Y. Tam, T. Fuehrmann, N. Mitrousis, M. S. Shoichet, *Neuropsychopharmacology* **2014**, *39*, 169.
[152] B. Gimi, T. Leong, Z. Gu, M. Yang, D. Artemov, Z. M. Bhujwalla, D. H. Gracias, *Biomed. Microdevices* **2005**, *7*, 341.
[153] H. Ye, C. L. Randall, T. G. Leong, D. A. Slanac, E. K. Call, D. H. Gracias, *Angew. Chem., Int. Ed.* **2007**, *46*, 4991.
[154] B. Gimi, D. Artemov, T. Leong, D. H. Gracias, W. Gilson, M. Stuber, Z. M. Bhujwalla, *Cell Transplant.* **2007**, *16*, 403.
[155] J. Wang, M. Patel, D. H. Gracias, *Nano* **2009**, *04*, 1.
[156] C. L. Randall, A. Gillespie, S. Singh, T. G. Leong, D. H. Gracias, *Anal. Bioanal. Chem.* **2009**, *393*, 1217.
[157] C. L. Randall, Y. V. Kalinin, M. Jamal, A. Shah, D. H. Gracias, *Nanomedicine* **2011**, *7*, 686.
[158] C. L. Randall, Y. V. Kalinin, M. Jamal, T. Manohar, D. H. Gracias, *Lab Chip* **2011**, *11*, 127.
[159] A. Azam, K. E. Laflin, M. Jamal, R. Fernandes, D. H. Gracias, *Biomed. Microdevices* **2011**, *13*, 51.
[160] J. Park, Y. V. Kalinin, S. Kadam, C. L. Randall, D. H. Gracias, *Artif. Organs* **2013**, *37*, 1059.
[161] G. W. Dahlmann, E. M. Yeatman, *Electron. Lett.* **2000**, *36*, 1707.
[162] D. Joung, K. Agarwal, H. R. Park, C. Liu, S. H. Oh, J. H. Cho, *Adv. Electron. Mater.* **2016**, *2*, 1500459.
[163] C. Liu, J. Schauff, D. Joung, J. H. Cho, *Adv. Mater. Technol.* **2017**, *2*, 1700035.
[164] K. Agarwal, C. Liu, D. Joung, H. R. Park, S. H. Oh, J. H. Cho, *Sci. Rep.* **2017**, *7*, 2680.
[165] K. Agarwal, C. Liu, D. Joung, H. R. Park, J. Jeong, D. S. Kim, J. H. Cho, *ACS Photonics* **2017**, *4*, 2436.
[166] J. H. Cho, S. Hu, D. H. Gracias, *Appl. Phys. Lett.* **2008**, *93*, 043505.
[167] D. Gracias, J. H. Cho, S. Hu, *MRS Online Proc. Libr.* **2010**, *1249*, 1249.
[168] P. Anacleto, E. Gultepe, S. Gomes, P. M. Mendes, D. H. Gracias, *Technology* **2016**, *04*, 120.
[169] J. S. Randhawa, S. S. Gurbani, M. D. Keung, D. P. Demers, M. R. Leahy-Hoppa, D. H. Gracias, *Appl. Phys. Lett.* **2010**, *96*, 191108.
[170] J.-H. Cho, M. D. Keung, N. Verellen, L. Lagae, V. V. Moshchalkov, P. Van Dorpe, D. H. Gracias, *Small* **2011**, *7*, 1943.
[171] D. Joung, T. Gu, J. H. Cho, *ACS Nano* **2016**, *10*, 9586.
[172] D. Joung, A. Nemilentsau, K. Agarwal, C. Dai, C. Liu, Q. Su, J. Li, T. Low, S. J. Koester, J. H. Cho, *Nano Lett.* **2017**, *17*, 1987.
[173] D. Joung, D. Wratkowski, C. Dai, S. Lee, J. H. Cho, *J. Visualized Exp.* **2018**, *139*, e58500.
[174] C. Dai, K. Agarwal, J. H. Cho, *ACS Nano* **2018**, *12*, 10251.
[175] C. Dai, J. H. Cho, *Nano Lett.* **2016**, *16*, 3655.
[176] H. R. Kwag, J. H. Cho, S. Y. Park, J. Park, D. H. Gracias, *Faraday Discuss.* **2016**, *191*, 61.
[177] R. Fernandes, D. H. Gracias, *Adv. Drug Delivery Rev.* **2012**, *64*, 1579.
[178] J. S. Randhawa, L. N. Kanu, G. Singh, D. H. Gracias, *Langmuir* **2010**, *26*, 12534.
[179] S. Pandey, N. Macias, C. Ciobanu, C. Yoon, C. Teuscher, D. Gracias, *Micromachines* **2016**, *7*, 78.
[180] J. Luo, X. Zhao, J. Wu, H. D. Jang, H. H. Kung, J. Huang, *J. Phys. Chem. Lett.* **2012**, *3*, 1824.
[181] V. B. Shenoy, D. H. Gracias, *MRS Bull.* **2012**, *37*, 847.
[182] Y. Chen, F. Guo, A. Jachak, S.-P. Kim, D. Datta, J. Liu, I. Kulaots, C. Vaslet, H. D. Jang, J. Huang, A. Kane, V. B. Shenoy, R. H. Hurt, *Nano Lett.* **2012**, *12*, 1996.
[183] D. Parviz, S. D. Metzler, S. Das, F. Irin, M. J. Green, *Small* **2015**, *11*, 2661.
[184] R. Bari, D. Parviz, F. Khabaz, C. D. Klaassen, S. D. Metzler, M. J. Hansen, R. Khare, M. J. Green, *Phys. Chem. Chem. Phys.* **2015**, *17*, 9383.
[185] Q. Liu, Y. Gao, B. Xu, *Appl. Phys. Lett.* **2016**, *108*, 141906.
[186] W. Xu, K. S. Kwok, D. H. Gracias, *Acc. Chem. Res.* **2018**, *51*, 436.
[187] J. D. Paulsen, *Annu. Rev. Condens. Matter Phys.* **2019**, *10*, 431.